**Master Thesis**

Karin van Minnen
Student nr: 5644720
August 2024

# A 3D Neuromusculoskeletal Model with Reflex-Based Controllers for Predictive Simulation of the Sit-to-Stand Motion of Unilateral Transfemoral Amputees

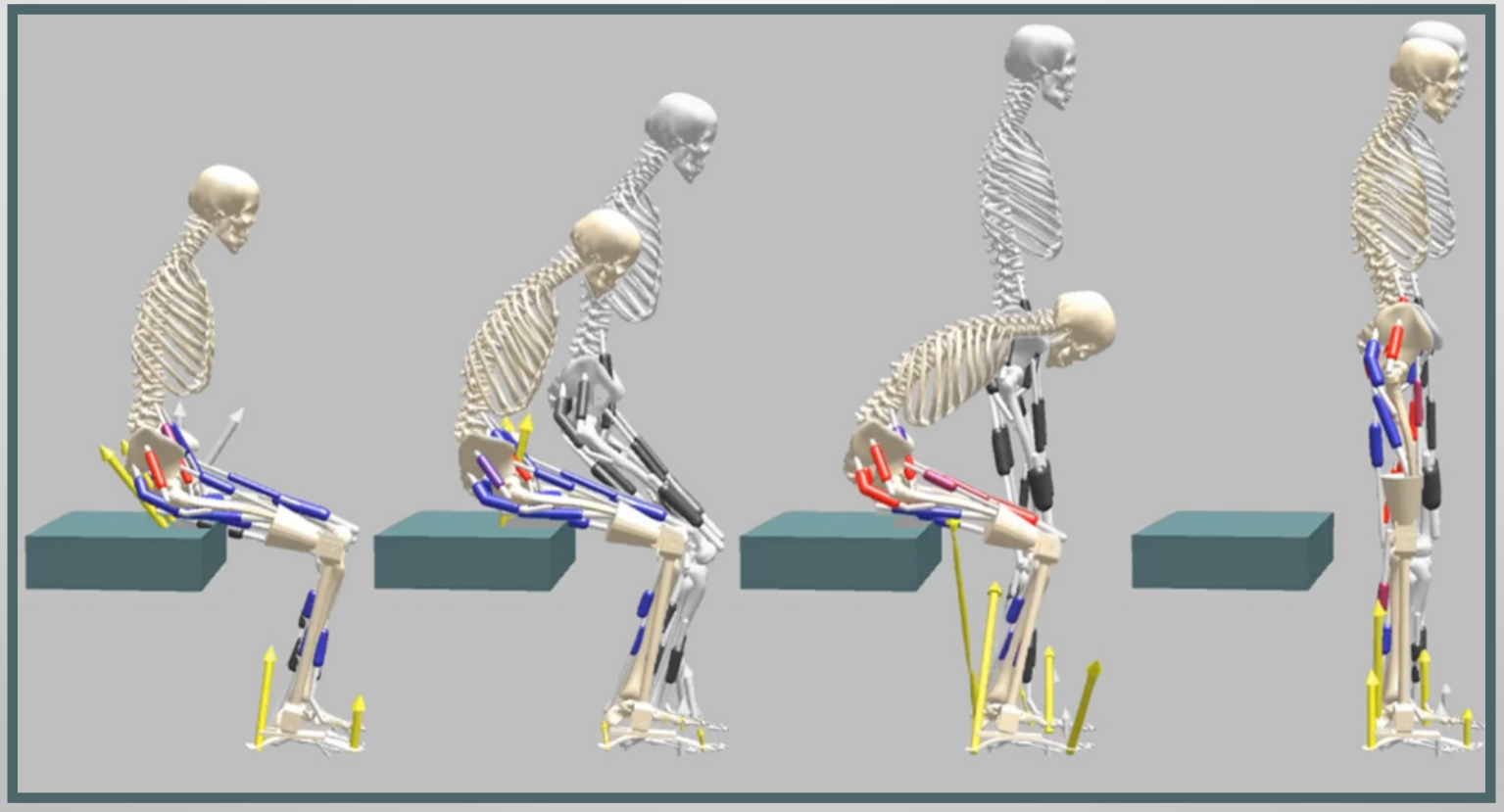

Delft University of Technology
Department of Biomechanical Engineering
Supervisors: Eline van der Kruk & Bob van der Windt

TU Delft

*MSc Thesis, ME51035,*
*K.S. van Minnen,*
*Student number: 5644720*

*Department of Biomechanical Engineering,*
*Delft, The Netherlands,*
*August 4, 2024*

# A 3D Neuromusculoskeletal Model with Reflex-Based Controllers for Predictive Simulation of the Sit-to-Stand Motion of Unilateral Transfemoral Amputees

Karin van Minnen

***Abstract*—Transfemoral prosthesis users typically perform the sit-to-stand motion unilaterally, placing minimal load on the prosthetic side. This increases the risk of injury and accelerates the degeneration of the intact limb. To address this, understanding compensation strategies is essential. Predictive neuromusculoskeletal modeling offers a method to investigate this. The aim of this study was to develop and validate a neuromusculoskeletal model with reflex-based muscle control to simulate the sit-to-stand motion in non-amputees and transfemoral amputees with a passive prosthesis. We developed a three-dimensional sit-to-stand musculoskeletal model of a non-amputee (20 degrees of freedom, 24 muscles) and a transfemoral amputee (20 degrees of freedom, 19 muscles), both incorporating a two-phase stand-up controller based on an existing two-dimensional reflex controller. We compared the simulation framework to measured kinematics, muscle activations, ground reaction forces, and existing literature on degrees of asymmetry and muscle forces. The developed framework was used to optimize prosthetic knee and ankle stiffness and damping for the sit-to-stand motion with a passive prosthesis. The simulated kinematics of the non-amputee matched measured kinematics. The prosthesis model indicated compensation strategies involving increased thoracic and lumbar extension, lumbar bending towards the non-amputated side, increased pelvic tilt combined with decreased hip flexion, and heightened muscle activation and force. Optimization results suggested a knee stiffness of 0.1432 [Nm/deg] and damping of 0.0246 [Nm·s/deg], while the ankle required a stiffness of 0.1968 [Nm/deg] and damping of 0.1350 [Nm·s/deg]. These values are recommended for testing in future experiments.***

## I. Introduction

Worldwide, an estimated forty million individuals in the developing world have an amputated limb, according to the World Health Organization [1], with 90% of new amputations affecting the lower extremity [2]. Major lower extremity amputation is predominantly linked to peripheral artery disease, often exacerbated by factors such as diabetes, cardiovascular diseases, and age-related risks [3, 4]. Diabetes increases the risk of amputation over twenty times [5], resulting in a lower limb being amputated somewhere in the world every thirty seconds [6].

An amputation significantly alters an individual's life, not only affecting their physical abilities but also their social interactions [7]. Prostheses play an important role in improving the quality of life for amputees [8], aiding in daily activities and boosting self-esteem [9]. However, prosthetic mobility is often more demanding [10], and long-term use may lead to secondary physical afflictions such as osteoarthritis, significantly affecting users' well-being [11].

The author is with the Delft University of Technology k.s.vanminnen@student.tudelft.nl

Among all routinely undertaken daily activities, the standing-up motion occurs approximately sixty times a day for most individuals [12] and is considered the most mechanically demanding motion [13]. This motion consists of three phases: leaning forward (P1), the transfer phase during which the seat-off occurs and the rising from the chair begins (P2), and the extension phase where balance is achieved (P3) (Figure 1). For transfemoral amputees (TFAs), this motion is particularly challenging because it requires not only an artificial ankle, foot, and part of a shank but also a knee joint. This challenge is enhanced by the fact that most (passive) prostheses lack the capability to supply energy to assist the user [14], requiring compensatory approaches to manage the motion [15, 16], changes in reinforcement schemes (such as prioritizing stability and pain avoidance over velocity due to fear of falling [16]), and alterations in sensory input (Figure 2). Due to the challenges involved in the transitional movement, the rising motion is often performed as a one-legged task with increased stress on the intact limb [17]. To help this group maintain independence and improve their quality of life, optimizing the stiffness and damping of a prosthesis to improve support of the standing-up motion could be a beneficial solution.

To address this, it is important to understand compensation strategies used by amputees. Predictive simulations offer a powerful tool for this purpose, allowing researchers to predict how amputees adapt their motion. Using feedback control models that incorporate control policies based on neural control principles, human movement can be accurately predicted and simulated. The first robust gait controller using limited proprioceptive feedback loops [19] laid the foundation for a predictive controller simulating sit-to-walk movement, which incorporates delayed proprioceptive feedback from muscle length, force, velocity, upper-body orientation (vestibular feedback), and monosynaptic and antagonistic feedback pathways [18]. While these models are designed for two-dimensional simulations, sufficient for symmetric models, modeling a transfemoral amputee requires consideration of asymmetry effects and therefore needs modeling in the third dimension.

Therefore, the objective of this study was to develop and validate a three-dimensional neuromusculoskeletal model for sit-to-stand (STS) motions with reflex-based muscle control, applicable to both non-amputees and transfemoral amputees. Kinematics, ground reaction forces (GRF), and muscle activation patterns recorded by van der Kruk et al. [20] served as benchmarks for the non-amputee simulations, while the prosthesis model was primarily compared with the non-

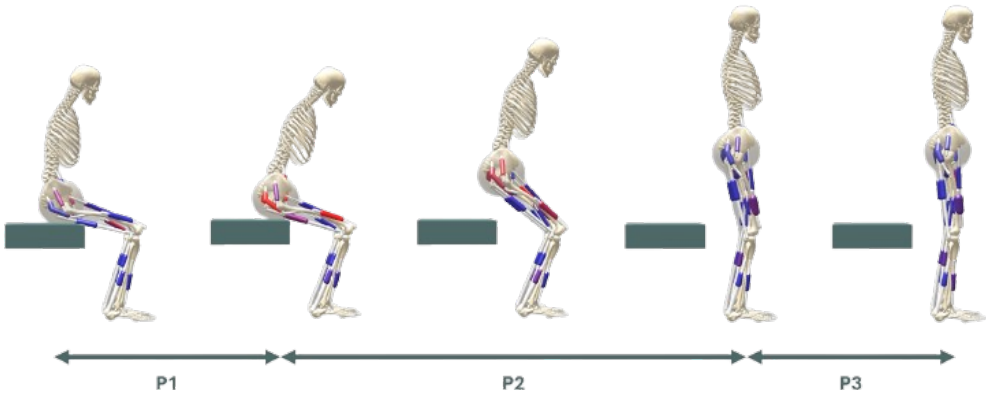


Fig. 1: Phases of the sit-to-stand motion: P1 defines the leaning forward phase, P2 the standing up phase, and P3 the balancing phase.

amputee model and literature values. This framework aimed to predict motion and simulate compensation strategies during STS, optimizing stiffness and damping parameters of passive prosthetic knee and ankle joints. This research intends to improve the independence of prosthesis users by improving the understanding of compensation strategies and by optimizing prosthetic design properties. Future experimental validation using real prostheses could further improve these findings. To our knowledge, this is the first three-dimensional neuromusculoskeletal model incorporating reflex-based muscle control, facilitating predictive simulations of the STS movement for both non-amputees and transfemoral prosthesis users. This marks a significant step toward optimizing parameters for the STS motion in transfemoral amputees.

## II. Methods

The STS controller used for simulation consisted of a two-phase reflex stand-up controller for both the baseline model (BM) and the prosthesis model (PM), based on the study by van der Kruk and Geijtenbeek [18]. The controllers integrated proprioceptive and vestibular feedback, along with constant excitation with distinct parameters for each phase (P1 and combined P2 and P3 of Figure 1). The free parameters were optimized to minimize muscle activation and overall effort [21], ensure stable motion, and avoid excessive ligament stress. Iterative optimizations were conducted, building upon the best results from parallel runs. The outcomes were compared to experimental data of non-amputees in which young male participants were asked to stand up and sit down while kinematics and muscle activation were recorded and biomechanical models were used to estimate joint kinetics [20]. This way, the BM could be validated and used as a comparison for the PM. All simulations and optimizations were executed in SCONE, version 2.3.1.2903 [22], using the Hyfydy simulation engine, version 1.6.0.1116 [23].

### A. Musculoskeletal Model

The two-dimensional musculoskeletal model of van der Kruk and Geijtenbeek [18] was used as the initial setup for the BM. This model represents a 1.80 [m] tall adult male with a mass of 75 [kg]. Adjustments to this model were made to convert it to a 3D model, resulting in a model with a total of twenty degrees of freedom (DoFs): six between the pelvis and ground, three rotational DoFs at each of the hips, one at each of the knees and ankles, a lumbar joint, with torque-driven control, between the pelvis and the lumbar allowing for three types of rotations, and one thoracic joint, also torque-driven, between the lumbar and the torso allowing thoracic extension (Figure 3).

The BM, consisting of 24 muscle-tendon units (MTUs), was adapted to represent a unilateral transfemoral amputee. In the PM, the left lower limb was adjusted to represent the prosthesis. For this, the tibialis anterior (TA), gastrocnemius (GAS), soleus (SOL), vasti (VAS), and biceps femoris short head (BFSH) were removed. The rectus femoris (RFEM) and hamstrings (HAM) were then reattached to the distal end of the residual femur, as previously done in the model of Raveendranathan and Carloni [24]. Specifically, the reattachment of the HAM is based on the attachment of the biceps femoris long head of Raveendranathan and Carloni [24]. The psoas (PSOAS), iliacus (ILIAC), gluteus maximus (GMAX), gluteus medius (GMED), and adductor magnus (ADDMAG) remain unchanged (Figure 3).

For the reattached muscles, a myodesis technique is assumed, meaning that muscles are sutured to the bone. However, this technique lacks a single standard method [25], with insufficient evidence to support current surgical choices [26]. Nevertheless, tendons can hold sutures well, while muscles do not [27]. Therefore, the optimal fiber length in the musculoskeletal model was kept identical to that of the BM, and the tendon slack length was adjusted. The decrease in tendon slack length was based on the total shortening of the muscle by comparing the muscle-tendon length of both sides (Appendix A). This decrease was then applied to the tendon slack length, resulting in the values of Table I. The maximum isometric force was kept the same because of the great variations within the literature about the muscle strength in the residual limb [28] (Table I). It should be kept in

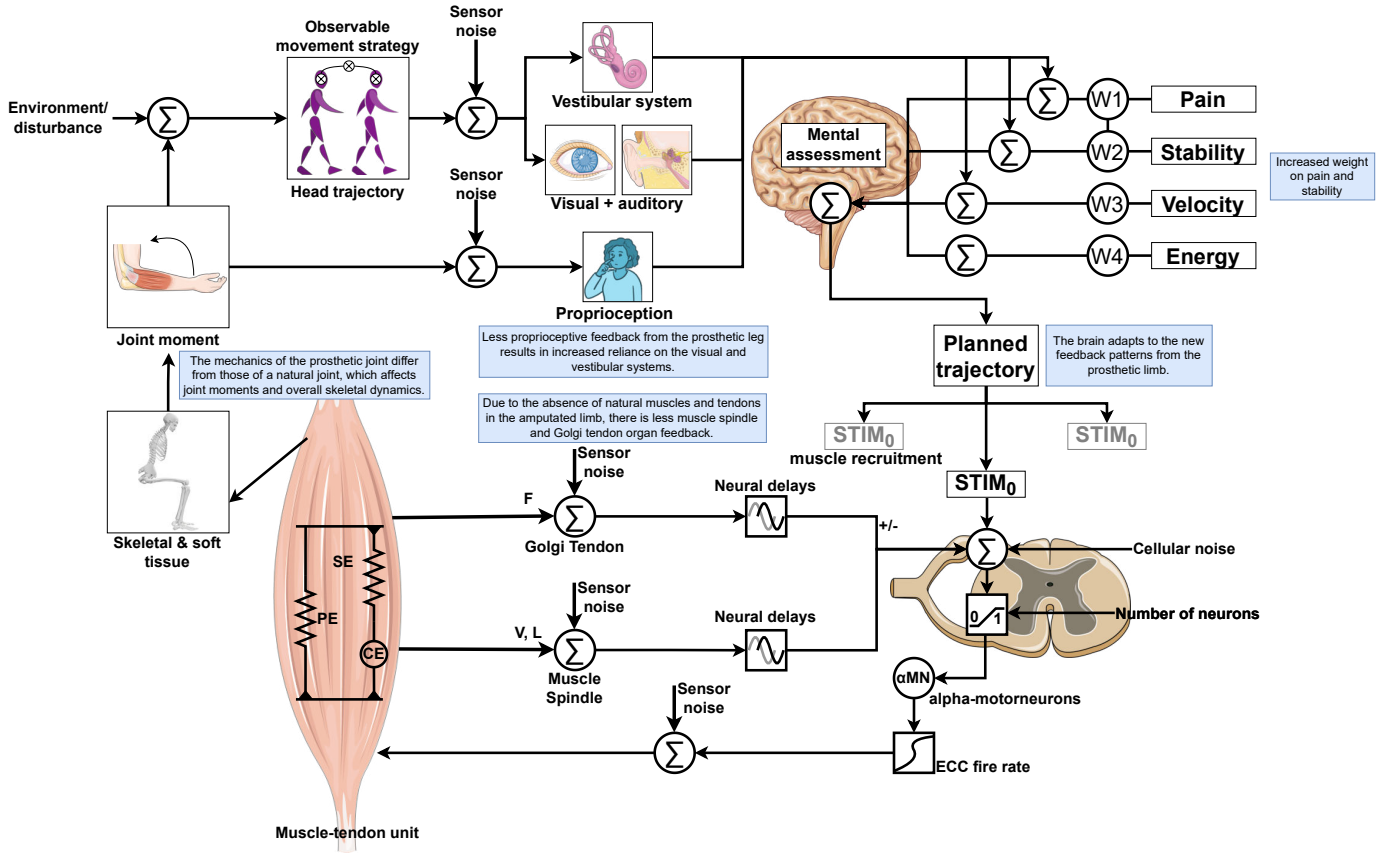


Fig. 2: Neuromuscular system feedback control, adapted from van der Kruk and Geijtenbeek [18]. In blue the parts of the neuromuscular system that are affected by prosthesis use [15, 16].

TABLE I: Muscle tendon parameters used in the musculoskeletal model.

| MTU in model | | Pathway | Tendon slack length [m] | Optimal fiber length [m] | Maximum isometric force [N] | Pennation angle at optimal fiber length [rad] |
|---|---|---|---|---|---|---|
| Psoas | Identical at both sides | lumbar-pelvis-femur-femur | 0.1970 | 0.1169 | 1113 | 0.215525 |
| Iliacus | Identical at both sides | pelvis-pelvis-femur-femur | 0.0934 | 0.1066 | 1073 | 0.279914 |
| Gluteus medius | Identical at both sides | pelvis-femur | 0.066 | 0.0733 | 2045 | 0.3578 |
| Gluteus maximus | Identical at both sides | pelvis-pelvis-femur-femur | 0.127 | 0.147 | 1944 | 0 |
| Adductor magnus | Identical at both sides | pelvis-femur | 0.06 | 0.087 | 2268 | 0.0872665 |
| Rectus femoris | Non-amputated side | pelvis-femur-tibia | 0.3050 | 0.1140 | 1169 | 0.087266 |
| | Amputated side | pelvis-femur | 0.174 | 0.1140 | 1169 | 0.087266 |
| Hamstrings | Non-amputated side | pelvis-tibia-tibia | 0.3250 | 0.0976 | 2594 | 0.202458 |
| | Amputated side | pelvis-femur | 0.1216 | 0.0976 | 2594 | 0.202458 |
| Vasti | Non-amputated side | femur-femur-tibia | 0.1230 | 0.0993 | 4530 | 0.063100 |
| Tibialis anterior | Non-amputated side | tibia-tibia-calcaneus | 0.2230 | 0.0980 | 1759 | 0.087266 |
| Soleus | Non-amputated side | tibia-calcaneus | 0.25 | 0.05 | 3549 | 0.436332 |
| Biceps femoris short head | Non-amputated side | femur-tibia-tibia | 0.1000 | 0.1103 | 804 | 0.214675 |
| Gastrocnemius | Non-amputated side | femur-calcaneus | 0.3900 | 0.0510 | 2241 | 0.172788 |

mind that this might lead to an overestimation of muscle forces [29, 30]. For the other muscles, the same properties were used as in the model of van der Kruk and Geijtenbeek [18], which are based on Gait2392 [31], for which the peak forces were summed to obtain values for the simplified model, and on Rajagopal et al. [32] for the HAM, BFSH, ILIAC, and PSOAS. The ADDMAG and GMED muscles added to the 3D model have muscle properties based on a previously designed 3D model included in the Hyfydy examples [23]. An overview of the MTUs parameters is presented in Table I.

In the PM, the prosthesis was simulated by adjusting the mass and inertia properties of the left femur, tibia, and calcaneus to replicate a realistic transfemoral prosthesis. Table II provides an overview of these values, and a different geometry file for prosthetic visualization has been inserted. Additionally, knee and ankle joints have been modeled by adding a joint motor in the Hyfydy file for the prosthetic knee and ankle, similar to how the lumbar and thorax joints have been defined. The stiffness and damping parameters of these prosthetic joints are optimized during simulation by incorporating an optimizer function in the SCONE file.

### *B. SCONE Implementation*

A simulation framework was developed using the open-source software SCONE: Simulated Controller OptimizatioN Environment [22]. The contact forces between the feet

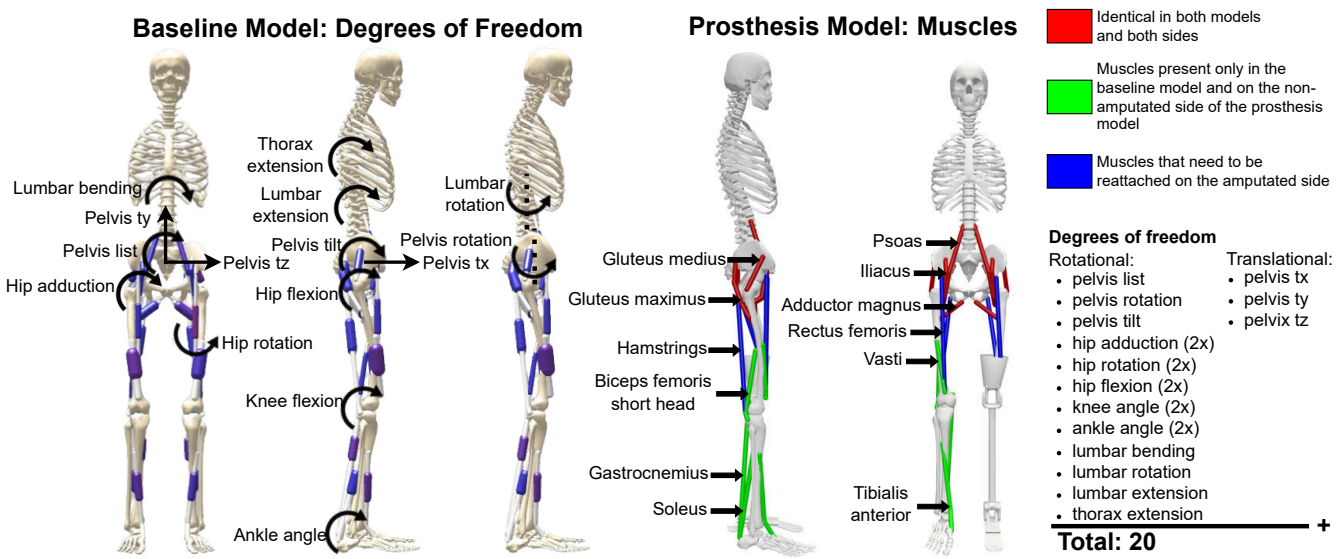


Fig. 3: Overview of BM and PM, with the twenty DoFs indicated in BM and the anatomy of the muscles used in the PM, highlighting the differences with the BM model.

TABLE II: Summary of the mass and inertia properties of the non-amputated leg and prosthetic leg. Further details regarding the calculation of these values are provided in Appendix B.

| | Mass [kg] | Inertia [kg·m$^2$] |
|---|---|---|
| Non amputated femur | 9.3014 | x = 0.1339 y = 0.0351 z = 0.1412 |
| Residual femur + upper leg prosthesis | 6.1507 | x = 0.08034 y = 0.02106 z = 0.08472 |
| Non amputated tibia | 3.7075 | x = 0.0504 y = 0.0051 z = 0.0511 |
| Prosthetic lower leg part | 1.5 | x = 0.02042 y = 0.00207 z = 0.02068 |
| Non amputated foot | 1.25 | x = 0.0014 y = 0.0039 z = 0.0041 |
| Prosthetic foot | 0.75 | x = 0.00084 y = 0.00234 z = 0.00246 |

and ground were adjusted slightly compared to the model by van der Kruk and Geijtenbeek [18] due to the conversion to 3D. The changes include the addition of an extra Hunt Crossley force sphere at the toes, resulting in one sphere with a radius of 3 [cm] at the heel and two spheres with a radius of 2 [cm] at the toes. Additionally, the buttocks contact geometry was changed to a capsule shape with a radius of 12 [cm] and length of [12] cm, based on Geijtenbeek [23], while the position was kept the same as in van der Kruk and Geijtenbeek [18]. For the PM, the prosthetic foot was modeled as a capsule with a radius of 3 [cm] and length of 22 [cm], approximating a rigid prosthetic foot. Other aspects remained unchanged, with the dissipation coefficient set to 1 [s/m], static friction at 0.9, dynamic friction at 0.6, and ligaments represented by joint forces with a limit stiffness of 500 [N/m].

### C. Controllers

The STS motion was simulated using a reflex controller with two phases. The reflex controller is based on monosynaptic and antagonistic proprioceptive feedback from the muscles, in which the monosynaptic part ensures rapid communication between muscle spindles and motor neurons in the spinal cord [33]. It triggers the stretch reflex, helps to maintain muscle tone and prevents overstretching while the antagonistic part ensures coordination between muscles in antagonistic pairs; sensory receptors in one muscle group inhibit the antagonist and facilitate the agonist muscle, ensuring smooth movement and efficient muscle activation. Additionally, the reflex controller, linked to the pelvis tilt, incorporates vestibular feedback. Furthermore, neural latencies were included, representing the time delay between the initiation of a sensory stimulus and the corresponding motor response [34]. Shorter latencies typically indicate faster reflex responses and are generated entirely by spinal circuits, while longer latencies take longer and involve regions above the spinal cord [35].

The STS controller is similar to the stand-up controller of van der Kruk and Geijtenbeek [18]. The controller's gains and the constant actuation were optimized, while the length offset was fixed at 1. Torque-driven lumbar and thoracic joints were controlled using PD control based on joint velocity and position. The delays added to the system were unchanged compared to the implementation by van der Kruk and Geijtenbeek [18], except for the addition of the 3D muscles: GMED and ADDMAG. Reflex controllers for the GMED and ADDMAG were added based on muscles with similar neural path lengths, resulting in the values shown in Table III. The GMED and ADDMAG were set to be each other's antagonists in the antagonistic part of the controller. The vestibular delay was kept the same as in van der Kruk and Geijtenbeek [18], computed based on electromyographic responses and adjusted for inter-muscular differences. Lumbar and thoracic joint delays were estimated considering central delay and conduction velocity estimates. Furthermore, controllers for the two additional DoFs in 3D at the lumbar joint, lumbar bending and lumbar rotation, were added, similar to the one for lumbar extension. The transition time between the reflex controllers was treated as a free parameter and incorporated into the optimization process. The PM used a similar controller setup but had its own set of initial conditions.

TABLE III: Neural latencies as implemented by van der Kruk and Geijtenbeek [18] for the monosynaptic, antagonistic, and vestibular controllers, with additions for the ADDMAG and GMED muscles included in the 3D model.

| Muscle | Monosynaptic control $\Delta_t$ [ms] | Antagonists | Antagonists control $\Delta_t$ [ms] | Vestibular control $\Delta_t$ [ms] |
|---|---|---|---|---|
| HAM | 15 | RFEM, VAS | 20 | 45 |
| BFSH | 20 | RFEM, VAS | 20 | 45 |
| GMAX | 10 | ILIAC, PSOAS | 10 | 40 |
| GMED | 10 | ADDMAG | 10 | 40 |
| ADDMAG | 10 | GMED | 10 | 40 |
| ILIAC | 10 | GMAX | 10 | 40 |
| PSOAS | 10 | GMAX | 10 | 40 |
| RFEM | 20 | HAM, BFSH | 20 | 45 |
| VAS | 20 | HAM, BFSH | 20 | 45 |
| GAS | 35 | TA | 35 | 55 |
| SOL | 35 | TA | 35 | 55 |
| TA | 35 | GAS, SOL | 35 | 55 |
| Lumbar | | | | 35 |
| Thoracic | | | | 30 |

### *D. Optimization Framework*

The equations of motion and their integration were executed in SCONE. Simulations commenced with an initial posture of the model's DoFs and velocities set to 0. This initial position, resembling common seating postures before standing up, was chosen to align with van der Kruk and Geijtenbeek [18]. Simulations terminated either upon reaching the maximum simulation time of 5 [s] or when the model fell, defined as the center of mass height dropping below 85% of its initial height. The optimization aimed to minimize the objective function, which comprised the following terms:

- Task term: Ensures the standing-up motion by forcing the pelvis y-direction to reach a minimum height of 0.88 [m].
- Energy term: Estimating energy consumption during standing up, combining metabolic energy expenditure [21] with the minimization of cubed muscle activations and torque at the lumbar and thoracic joints.
- Penalize unnatural joint states: Prevents lumbar extension, thorax extension, pelvis tilt, hip adduction, and ankle angle from entering unnatural states.
- Prevent overstretching of the knee: Knee extension is limited to 5 [deg] for both knees in the BM. For the PM, this term was only applied to the non-amputated side, because prosthesis users are taught to completely stretch their prosthetic knee to lock it during balance.

When a suitable solution was found, all terms in the objective function for the BM became zero except for the energy term, which then became the sole objective to minimize. Since the unnatural joint states term required limits that are not exactly known for prosthesis users and to prevent forcing the simulation too much in a human-defined direction, the terms that penalize unnatural joint states and knee overstretching were removed after a balanced motion was achieved. This adjustment ensured that also PM could solely focus on energy minimization.

For the optimizations, the Covariance Matrix Adaptation Evolutionary Strategy (CMA-ES) within the open-source software SCONE was used, with multiple parallel optimizations starting from the same initial guesses. The best result from each batch was used for the subsequent optimization round. Initially, for the BM, the reflex controllers from van der Kruk and Geijtenbeek [18] served as the starting point in the first optimization batch. Subsequently, for the PM, the initial values were based on the optimized results of the BM. Both the BM and PM used the same SCONE setup, differing only in the PM's additional optimization of prosthetic knee and ankle parameters via a function that calculates the optimal stiffness and damping values for each simulation and an initial displacement constraint for the prosthetic foot. The displacement constraint for the prosthetic foot was added because initially, the PM exhibited a standing-up motion where the prosthetic leg was lifted, which corresponds to the reality where the rising motion is often performed as a one-legged task [17]. However, the goal of this study was to simulate standing up in the manner taught in rehabilitation clinics: using both legs and to determine suitable prosthetic properties for this purpose. To address simulations where the model stood up using only one leg and to avoid convergence to undesired local minima, a custom ScriptMeasure was implemented for the prosthetic foot. This measure minimizes differences in horizontal and vertical foot positions at each time step to keep the prosthetic foot on the ground (details in Appendix H). Once suitable initial conditions for the controller were established, these ScriptMeasures became unnecessary and were subsequently removed.

### *E. Validation*

For validation, the emphasis was on the BM, with the assumption that if this is valid, the PM should be relatively reliable as well, due to the similar optimization framework.

*1) Baseline Model Validation:* The results of the BM's STS simulation were compared to the kinematic and kinetic experimental data of eight young males [20], as the musculoskeletal model represents a male without accounting for muscle aging properties. Each participant performed the STS motion and sitting down task three times while instructed to not use the arms. Force plate data were captured using two Kistler force plates in both the chair and the ground, while 16 EMG sensors and 84 reflective markers captured the EMG signals of certain muscle groups and the motion, respectively. The BM was compared to the joint angles of the experimental data and the GRF; when this comparison showed overlap, the BM was considered useful for comparison with the PM. Additionally, Caruthers et al. [36] used experimental STS data from seven young healthy participants as input for their custom 3D musculoskeletal model in OpenSim, ultimately determining muscle forces. This validated data was also used to check the validity of the developed model in terms of muscle forces.

*2) Prosthesis Model Validation:* The PM was primarily compared to the validated BM under the assumption that, given their similar setups and the BM's alignment with experimental data, meaningful conclusions could be drawn. To assess the relevance of these findings in comparison to real prostheses, experimental data from Highsmith et al. [17] was used. This dataset comprised 21 unilateral transfemoral amputees using three different types of prosthetic knees (the active Power Knee of Össur [37], the semi-active C-Leg of Ottobock [38] and

the passive knee with hydromechanical components: Mauch SNS [39]), with recorded kinematic and kinetic data for the STS motion.

### F. Data Analysis

All data analysis was performed in MATLAB version R2022B; more information about the used MATLAB framework can be found in Appendix G.

*1) STS Duration:* For data analysis, the duration of the total STS movement was normalized and subsequently analyzed. For normalization a clear definition was important to allow accurate comparison. The STS motion can be divided into three phases (P1, P2, P3) [40, 41] as illustrated in Figure 1. In the simulations, the end of the motion was determined when the pelvis y-position reaches a height of 0.93 [m] and remains stable for the subsequent 0.25 [s]. Once this criterion was met, the moment when stability was achieved, plus an additional 0.25 [s], was set as the end time, following Highsmith et al. [17]. Due to variations in participant heights during experiments, the end time of the experimental data was set to the time at which their maximum pelvis y-position minus 0.01 [m] was reached for 0.25 [s], thus accounting for potential noise. The simulation's start time, the start of P1, corresponded to the beginning of the simulation. However, in experimental data, this varied since participants do not always start moving immediately. Therefore, the definition used in this paper was based on the assumption that the ratio between seat-off and balance, and between the start and seat-off, remained constant. Therefore, if a subject took longer from seat-off to balance, they likely also took longer from initiation. This ratio was determined by the BM simulation as defined in Equation 1.

$$\text{Ratio P1} = 1 - \frac{\text{End time P3} - \text{Start time P2}}{\text{End time P3 - Start time P1}} \tag{1}$$

The ratio of duration P1 was then applied to the experimental data, where the time of seat-off was accurately determined using force plate data. The time interval between the end and start of seat-off corresponded to a ratio as determined in the BM according to Equation 1, which was then used to calculate the start time of P1 for each individual participant and trial. For the visualization of results and analysis, the time for P1 was normalized to 100%, and the time after seat-off was also normalized to 100%, resulting in the entire motion corresponding to 200%.

*2) Degree of Asymmetry:* A comparison between BM and PM was obtained by examining the degree of asymmetry (DoA). To calculate the difference between both the prosthetic side and non-amputated side, DoA was calculated using Equation 2 based on Highsmith et al. [17], in which *S* indicates the sound side or the dominant side in the case of the control group, and *P* indicates the prosthetic side or non-dominant side for the control group. Since in simulation it is not possible to speak about a dominant side, the absolute value of the DoA was used for the BM. This DoA was calculated for the GRF and peak knee and hip joint moments.

$$DoA = \frac{S - P}{S + P} \times 100 \tag{2}$$

*3) Prosthesis Optimization Comparison:* During regular motion, the knee joint demonstrates a spring-like behavior [42]. Due to that behavior, an estimate of the optimal stiffness was determined by estimating the quasistiffness, the slope of the linear fit to the knee moment-angle curve [42]. This was done by using Equation 3, in which $k$ indicates the stiffness [Nm/deg], $\theta$ the knee angle [deg], and $M$ the corresponding moment [Nm]. Using this approach, insight into how much the optimized prosthetic knee in the simulations contributed compared to the sound knee and to a transfemoral powered knee that mimics non-amputated knee behavior [43] could be obtained.

$$M = k\theta \tag{3}$$

## III. Results

### A. Baseline Model

Figure 4 shows the joint angles over the whole STS motion, indicating that for the first phase of the STS motion, P1, all joint angles, except for the right knee angle and left hip adduction, have an overlap of 100% with the experimental data range. The right knee angle has an overlap of 95.0%. The left hip adduction angle has an overlap of 0%, indicating a clear mismatch. For the part of the motion after seat off, lumbar extension has an overlap of 15.8%, left hip flexion 97.0%, and hip adduction 93.1% and 70.3% for the left and right sides, respectively, while all other angles have 100% overlap. In terms of DoA in GRF (Figure 6), a value of 4.4% was found, which is within the range of the experimental data (5.7% $\pm$ 4.7%) and the non-amputee group of Highsmith et al. [17] (7% $\pm$ 9%). The DoA of the joint moments is 7.7% and 2.1% for the knee and hip, respectively, which is within the range for the knee moment of Highsmith et al. [17] who reported an asymmetry towards the non-dominant side of -3% $\pm$ 11%. The BM's hip moment asymmetry is lower compared to the 21% $\pm$ 10% reported by Highsmith et al. [17]. The peak muscle forces for the VAS, GMAX, and ADDMAG were within the range reported by Caruthers et al. [36], while the soleus muscle force was just above the range with a peak force of 309.5 [N].For the GAS, Caruthers et al. [36] reported 187.38 [N] $\pm$ 109.86 [N], but only included the medial gastrocnemius. Additionally, the BM's hamstrings peak force was higher than the single reported peak muscle force of the biceps femoris long head by Caruthers et al. [36] (885.5 [N] versus 490.06 [N] $\pm$ 380.64 [N]). Furthermore, the soleus muscle of the BM resulted in a higher muscle force (928.9 [N] versus 460.63 [N] $\pm$ 213.26 [N]), while the RFEM showed a lower force (397.3 [N] versus 944.03 [N] $\pm$ 382.21 [N]). Although Caruthers et al. [36] didn't report the exact values for the GMED, they mentioned that the unreported muscles produced forces less than 200 [N], which is significantly less compared to the GMED's force according to the BM, but within the range of the TA and BFSH (additional comparison about muscle activation can be found in Appendix C1).

### B. Compensation Strategies Transfemoral Amputee

*1) Joint Angles:* The BM showed increased lumbar extension (77 [deg] in PM versus 52 [deg] in BM) and thoracic

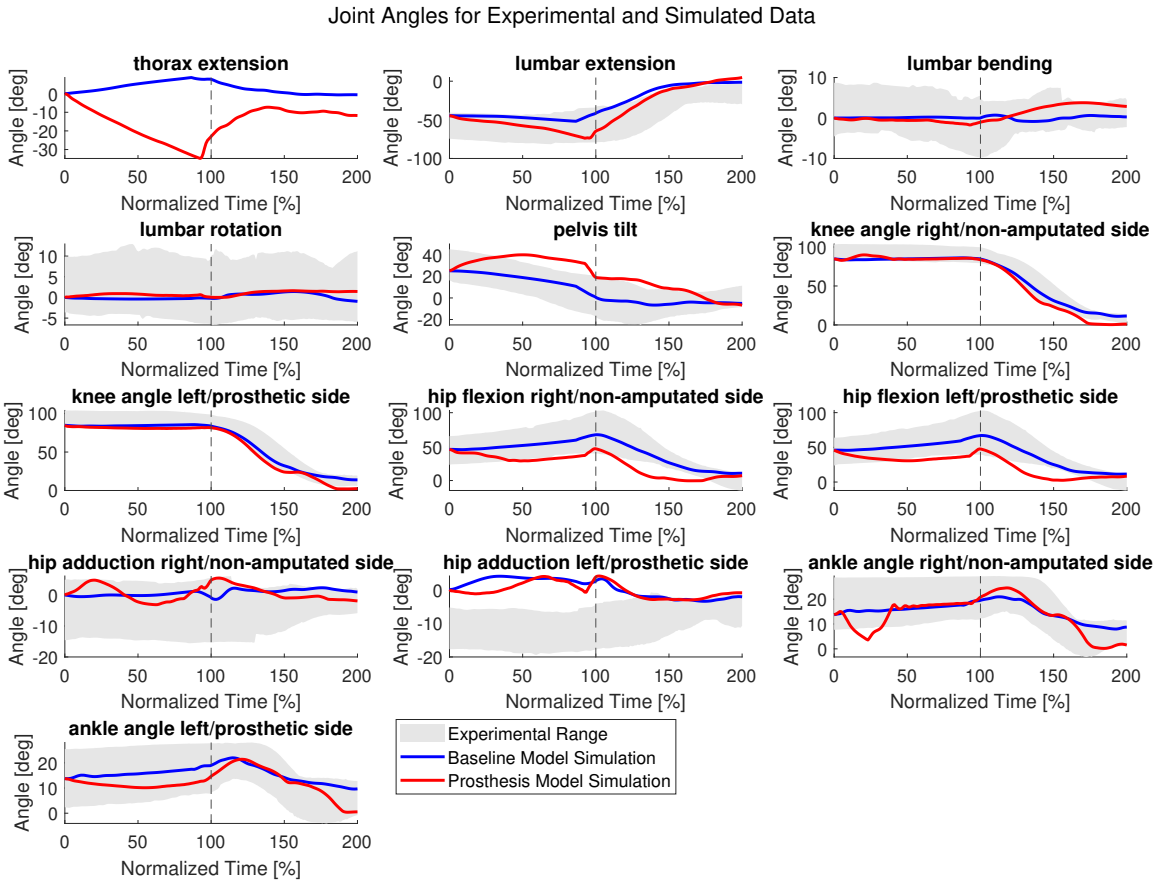


Fig. 4: Joint Angles during STS for BM versus PM. The shaded grey area represents the complete range of all experimental data (individual experimental joint angles can be found in Figure A.5). The black dotted line represents the seat-off moment.

extension (maximum extension of 33 [deg] for PM versus 8.7 [deg] flexion in BM) during P1, as illustrated in Figure 5. Additionally, during balance, both knees are completely extended. Moreover, lumbar bending and pelvis tilt vary over a wider range during STS, with the pelvis tilt ending in a similar position during balance (-4.65 [deg] in PM versus -5.0 [deg] in BM), while the lumbar remains slightly bent (end position of 2.9 [deg] in PM compared to 0.27 [deg] in BM) towards the non-amputated side. When examining the ankle angles, a more plantarflexed end position can be observed for both ankles (0.87 [deg] in the prosthetic ankle versus 9.67 [deg] in BM, while the other ankle shows -0.86 [deg] in PM versus 8.75 [deg] in BM) with a quick up-and-down movement of the non-amputated ankle during P1. A smaller hip flexion peak around seat-off indicates another difference between PM and BM, with the prosthetic side of PM reaching 47 [deg] for both sides, while BM reaches a peak of 67 [deg] for both sides. The final hip flexion position, on the other hand, shows a smaller difference, with PM being slightly more extended on both sides (a difference of 5.7 [deg] for the prosthetic side and 3.5 [deg] for the non-amputated side). The hip adductions on both sides show a similar pattern compared to the BM, with a mean difference over the whole motion of 1.56 [deg] for the prosthetic side and 1.23 [deg] for the non-amputated side.

*2) DoA:* In terms of DoA in GRF, PM shows a DoA of 14.75%, which is an increase compared to the BM (4.40%) while still being within the range of the non-amputee group of Highsmith et al. [17] (7% $\pm$ 9%), but outside the range of the experimental data of van der Kruk et al. [20] (5.72% $\pm$ 4.60%). Nevertheless, the PM shows a clear decrease in DoA of GRF compared to the best-scoring prosthesis on this aspect, the Power Knee, which has a DoA of 53% $\pm$ 14%, indicating that the prosthesis is being used during the stand-up motion (graph indicating the GRF over time can be found in Figure A.6). In contrast, the DoA of joint moments indicates that in terms of hip moment asymmetry, the PM performs asymmetrically towards the prosthetic side. This is in contrast with all the prostheses tested by Highsmith et al. [17], which perform asymmetrically towards the sound side. Nevertheless, the absolute value of hip asymmetry for the PM, at 32%, is close to the best-performing prosthesis reported by Highsmith et al. [17] in this aspect, the power knee (34% $\pm$ 16%). The asymmetry in knee moment, on the other hand, is 82.38% towards the sound side, which is lower than the results of

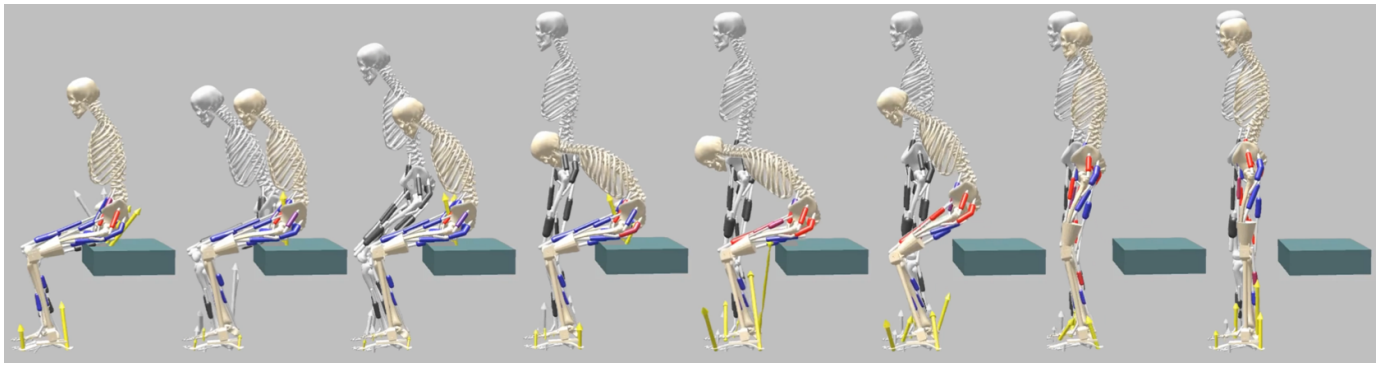

Fig. 5: Differences in motion between the BM (grey shaded model in the back) and the PM (in front).

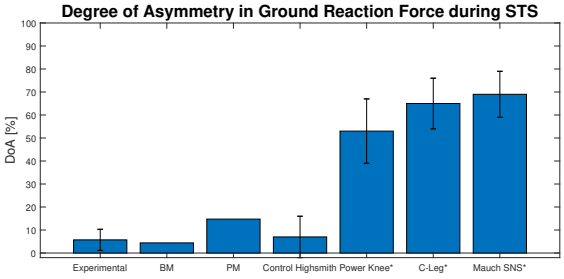


Fig. 6: DoA of the GRF of both the simulated BM and PM compared to experimental data of van der Kruk et al. [20] and the data of Highsmith et al. [17].
∗The data for the Power Knee, C-Leg, and Mauch SNS prostheses are all based on Highsmith et al. [17].

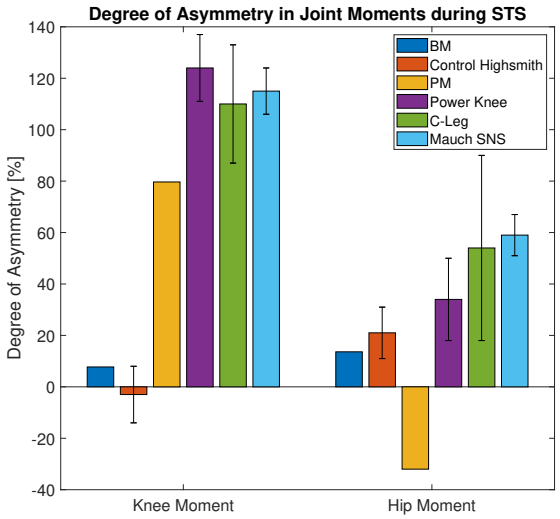


Fig. 7: Comparison of the DoA of knee and hip moments with prostheses from Highsmith et al. [17]. The data for the Power Knee, C-Leg, and Mauch SNS prostheses are all based on Highsmith et al. [17].

Highsmith et al. [17], but higher than the 7.73% of the BM. The absolute peak joint moments are visualized in Figure 8. Besides differences in the knees and hips, the lumbar extension moment of PM is 1.92 times higher than that of BM, and the thoracic extension increases by a factor of 2.62 for PM.

*3) Muscle Force & Activation:* The muscle activation of the PM (Figure A.3) indicates that higher muscle activation is required, even for balancing, compared to BM. The GMEDs, right GMAX, ADDMAGs, right ILIAC, and PSOAS of the PM remain fully activated at the end of the motion, while the HAMs and SOL show minimal activation but still produce force, as shown in Figure 9. The peak muscle forces illustrate clear differences between BM and PM for all muscles except GMAX (muscle force over time can be found in Figure A.4). The TA, GAS, VAS, BFSH, RFEM, PSOAS, ILIAC, GMED, and ADDMAG all show increased force in the muscles of the non-amputated side of PM compared to BM, while only the SOL and HAM of the non-amputated side show a decrease. The GMAX and GMED show similarity between both sides of the PM, with an increase of 3.12% and 1.83%, respectively, for the amputated side muscles. The ADDMAG and RFEM show a higher increase for the prosthetic side muscles with 23.25% and 30.30%, respectively, resulting in the RFEM of the amputated side reaching 1227 [N], exceeding the maximum isometric force of 1169 [N]. The HAM of the prosthetic side has a peak force of 1392 [N], which is 22.55 times higher than the non-amputated side HAM (61.7 [N]). The PSOAS and ILIAC are the only two muscles present on both sides that produce decreased force on the amputated side compared to the non-amputated side. The PSOAS on the non-amputated side has a peak force of 1420.78 [N], while the amputated side has a value of 1222.19 [N]; both values exceed the maximum isometric force of 1113 [N]. Additionally, the non-amputated side ILIAC has a peak force of 1369 [N], exceeding the maximum isometric force of 1073 [N], while the amputated side muscle is just below this value at 1012 [N].

*4) Duration:* The seat-off of BM occurs at 0.47 [s] while that of PM occurs at 1.28 [s], meaning that P1 takes 0.81 [s] longer for PM, while the end time differs 0.79 [s] (BM 1.18 [s] versus PM 1.97 [s]), indicating that the rest of the motion happens slightly faster for PM compared to BM.

### C. Optimization Prosthetic Parameters

The PM optimization resulted in a knee stiffness of 0.1432 [Nm/deg] and a damping of 0.0246 [Nm·s/deg] while

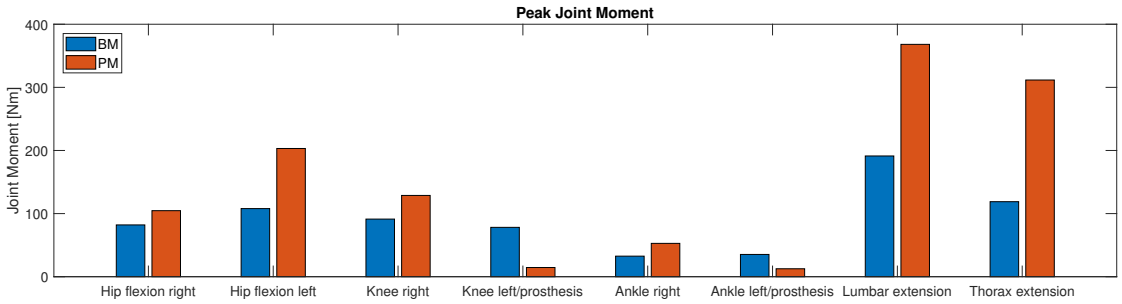


Fig. 8: Individual peak joint moments for both sides of the BM and PM. In the PM, the left leg is replaced by a prosthesis.

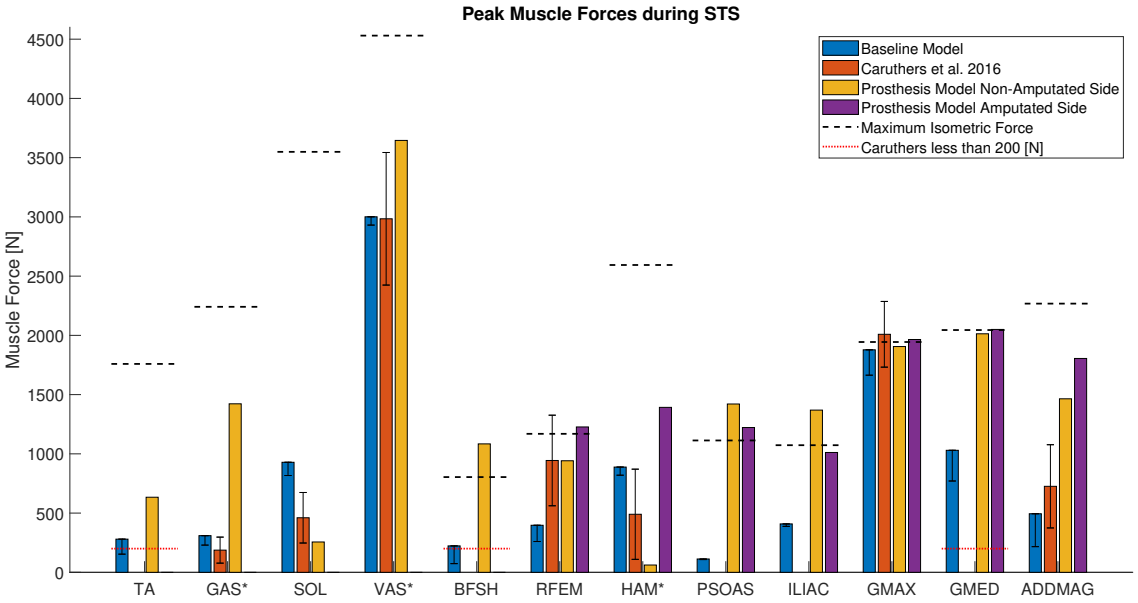


Fig. 9: Peak muscle forces for the BM (showing the peak of both sides with error bar indicating the difference) and PM compared with values reported by Caruthers et al. [36]. Caruthers et al. [36] did not provide data for all the muscles modeled for BM and PM, resulting in empty bars. Muscles that produced forces less than 200 [N] were not reported by Caruthers et al. [36]. Since Caruthers et al. [36] measured EMG data for the TA, biceps femoris, and GMED, but their forces were not discussed, it is assumed that they produced forces less than 200 [N].
∗The vasti represent the sum of vastus intermedius, vastus medialis, and vastus lateralis. The hamstring data from Caruthers et al. [36] includes only the biceps femoris long head, and the gastrocnemius data shows only the medial gastrocnemius.

the ankle stiffness was 0.1968 [Nm/deg] and a damping of 0.1350 [Nm·s/deg]. Figure 10 indicates that the found optimal knee stiffness matches the maxima of the knee-angle moment curve, but the value is lower than the optimal value of 1.1[Nm/deg] reported by Wu et al. [43] for a powered knee prosthesis that mimics the dynamic behavior of a non-amputated knee. Additionally, Wu et al. [43] reported a damping of 0.4 [Nm·s/deg] which is a factor 16 higher than the result of BM.

## IV. Discussion

### A. Baseline Model

This study demonstrated that a two-phase reflex-based neural controller can realistically simulate the task of standing up in three-dimensional space. The BM showed 100% overlap with the experimental data for seven out of twelve joint angles and over 96% overlap for three additional joints (right knee angle, left hip flexion and right hip adduction). However, lumbar extension and left hip adduction exhibited less accurate overlaps, at 57.5% and 35.5%, respectively, over the entire motion. The discrepancy in lumbar extension becomes noticeable around seat-off and is likely at least partially caused by the simplified model, where the buttocks are represented by a single capsule. In real life, contact with the chair lasts longer as the thighs roll off [18], leading to a more abrupt change in the lumbar extension angle before seat-off in the simulations. Additionally, the higher lumbar extension observed in the BM after seat-off, compared to the experimental data, may be partly due to the participants in the experiments knowing they had to sit down again, causing them to extend less.

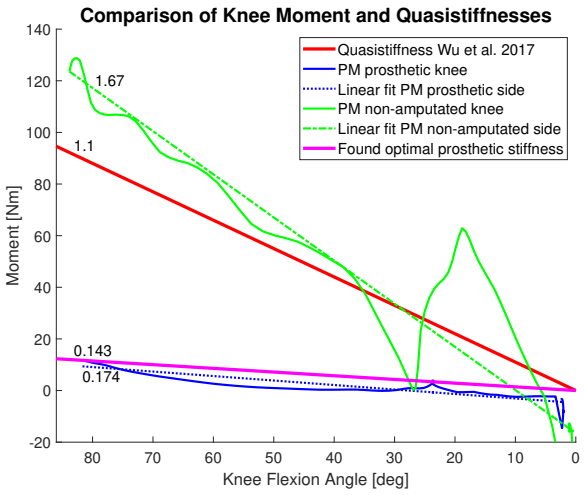


Fig. 10: The moment-angle (stiffness) curves of the STS motion from seat-off to stable standing for both the BM and PM with linear fits and their slopes, indicating stiffness, in Nm/deg for comparison.

Moreover, the BM represents a 1.80 [m] tall male weighing 75 [kg], which does not reflect the average characteristics of the experimental participants [20]. Despite the lower overlap percentage for lumbar extension, the model follows the general course of the motion and remains less than 5.5% above the maximum of the experimental data. The greater mismatch in left hip adduction is believed to be due to the experimental data errors rather than the model. Comparing the BM's left hip adduction with the experimental data for right hip adduction shows a 100% overlap throughout the entire motion.

While the model was compared to muscle force data from Caruthers et al. [36], it was not compared to all muscles due to limited data availability. The comparison indicated higher SOL force and lower RFEM force. This discrepancy may result from the optimization process within the framework, which can produce various movement strategies from identical initial scenarios. In addition Caruthers et al. [36] likely used different maximum isometric forces, resulting in other ratios between muscle forces. In this study, the strategy with the lowest cost was chosen; however, due to muscle redundancy, other plausible strategies are also possible. Therefore, future validation is recommended through either EMG measurements of experimental data combined with a validated model to estimate muscle forces, or by obtaining further information from the model of Caruthers et al. [36] to use similar values for maximum isometric force. The comparison with Caruthers et al. [36] also indicated that the forces of RFEM and GMAX of Caruthers et al. [36] were higher than the defined maximum isometric forces used in this study. For future work, the musculoskeletal model would benefit from improved estimates of these forces to enable more accurate comparisons.

### *B. Compensation Strategies Prosthesis Model*

The use of a transfemoral prosthesis requires compensation strategies for performing the STS movement, involving changes in both kinetics and kinematics. This study demonstrated that a two-phase, three-dimensional reflex-based controller, incorporating an adapted musculoskeletal model for a transfemoral prosthesis, can be used to identify these compensation strategies. The kinematic analysis revealed that initiating the movement requires additional momentum through increased thoracic and lumbar extension, often associated with lower back pain [44], as well as a greater pelvic tilt angle. This corresponds to the findings of Burger et al. [45], who reported that TFAs flex the trunk significantly more than non-amputees before seat-off and later lean more forward while bending increasingly toward the healthy side. This is consistent with the lumbar bending result showing a shift towards the non-amputated side. An increased inclination of the pelvis was also reported. Nevertheless, the finding by Burger et al. [45] that TFAs flex their hips to a greater extent was not observed in this study; the hip flexion peak actually reached a lower value while the end position was similar. Additionally, the PM showed highly extended knees, which in real life ensures that the prosthetic knee doesn't collapse during standing, allowing the user to put weight on it during balancing [45]. However, this also indicates a limitation: for non-amputees, the knee is always slightly flexed, as demonstrated by the BM and experimental data. In contrast, the non-amputated knee of the PM did not exhibit this characteristic. This discrepancy suggests different prioritizations between BM and PM, with the PM's knee extending after removing the measure that prevented this, in an effort to minimize overall effort. This highlights a disparity between the results. Furthermore, at the start of the PM simulation, a small up-and-down movement of the non-amputated foot occurred, which is not expected to be a compensation strategy. While more focus could have been placed on preventing this motion, the authors do not believe that this up-and-down movement influences the results of this study.

This study also compared the DoA of both GRFs and joint moments. The results showed that the PM had a clear decrease in the DoA of the GRF compared to the prostheses studied by Highsmith et al. [17]. However, it should be noted that the effective use of the prosthesis for standing up in real life also depends on user trust due to the absence of proprioception [46], which the simulation does not account for. Besides the DoA of the GRF, the DoA of the knee moment showed improvement compared to current prostheses. However, it remained more asymmetric than in non-amputees, indicating that the sound knee and the prosthetic knee are not equally contributing to the motion. This imbalance could potentially accelerate joint degeneration. Nonetheless, the results of this study were achieved solely by optimizing stiffness and damping parameters, which could improve the design of future passive prostheses, while Highsmith et al. [17] reported values for, in addition to a prosthesis with hydromechanical components, (active) microprocessor knees.

The DoA of the hip moment showed an unexpected and contradictory effect in terms of the direction of the asymmetry. The PM exhibited hip moment asymmetry towards the prosthetic side, unlike the prostheses tested by Highsmith et al. [17], which showed asymmetry towards the sound side.

The authors believe this discrepancy can be attributed to the optimization framework of this study. Initially, the PM was forced to keep both feet on the ground. By doing so, and by not accounting for the trust effect of prosthesis users in the simulation, the PM used the prosthesis to stand up. In contrast, Highsmith et al. [17] reported that in most cases, transfemoral amputees did not load their prosthesis extensively, resulting in a one-legged task.

Besides the DoAs, the peak joint moments showed that all non-prosthetic joints are experiencing higher peak moments, with the prosthetic joints producing decreased moments compared to the BM and the non-amputated side. While the DoA might be lower, the higher peak moments support the statement that TFAs have an increased risk of developing osteoarthritis in both the residual hip and intact lower-limb joints [30].

The increased difficulty of the STS task for transfemoral amputees is also evident in the muscle activations and muscle forces, where even the balancing task requires high activation. Additionally, the increased lumbar and thorax extension resulted in a prolonged P1, which corresponds with the findings of Burger et al. [45], who also found that TFAs have an increased time to seat-off. Nevertheless, Burger et al. [45] mainly found an increased time from seat-off to standing, while this phase happened slightly faster in the PM simulation, likely due to the optimization framework setup where the model needed to reach a certain height at a specified time. This means that if P1 takes longer, the model must increase its speed to meet the same requirement.

The high muscle activation during balance indicates that the balancing task itself is highly energy-intensive. The optimal fiber length was unchanged for the reinserted muscles, but for the HAM of the amputated side, this resulted in very low activation (Figure A.3) while still producing a force of 1392 [N], likely due to passive forces. Since this force exceeds half of the maximum isometric force, higher muscle activation was expected. Manual tuning has demonstrated that the reattached hamstrings can be effectively activated when both the tendon slack length and the optimal fiber length are modified (Appendix F). However, further research is required to fully understand these adjustments and their impact on muscle activation. Additionally, further comparison with EMG data and force data of both non-amputees and amputees can shed more light on the viability of these results. It is recommended to explore whether it is possible to decrease the high activations during balance. Investigating the effects of doubling all maximum isometric forces could provide interesting insights and prevent muscles from being completely activated.

Given that older adults frequently use their arms to assist in standing up [20], future research would benefit from incorporating arms into the model. This addition would enable simulations to include scenarios such as using armrests or pushing off from the thighs, potentially leading to different strategies and reduced peak joint moments and muscle forces.

### C. Optimization Prosthetic Parameters

The framework has proven useful for identifying suitable stiffness and damping values for prosthetic knees and ankles. The optimal stiffness found in this study differs from the stiffness recommended by Wu et al. [43], with a lower value for both prosthetic knee stiffness and damping. This is not surprising, as Wu et al. [43] reports the optimal value for a powered knee prosthesis that can closely mimic the STS motion of non-amputees, while the PM tries to mimic the same motion while only being able to change the spring and damping properties of the prosthesis. Interestingly, the average of the two linear fits for the knee-moment curves is close to the value reported by Wu et al. [43]. To improve the DoAs and the required joint moments and muscle forces, a higher value for the optimal stiffness was expected. Nevertheless, considering the benefit of having a passive prosthesis that assists with standing up, this study provides a good foundation for identifying such a value. Future experiments are recommended to test the suitability of the identified values in real-life prostheses. If future experiments validate these prosthetic values, the framework from this study could facilitate the rapid optimization of prosthetic settings. This includes, for example, identifying corresponding optimal settings for ankle stiffness and damping, as well as knee damping, given a certain knee stiffness. Which is especially interesting since mechanical properties of prostheses are often unknown [47, 48]. Additionally, the framework could be used to determine values for various amputation heights, evaluate the impact of different prosthetic mass and inertia properties, or consider alternative attachment points. Beyond the STS motion, it is also important to consider how the prosthetic parameters affect other aspects, such as sitting down and sit-to-walk.

### D. Limitations

Since simulations are simplified representations of reality, researchers should be mindful of several factors when interpreting the results.

- While this study presents the first three-dimensional neuromusculoskeletal model with reflex-based muscle control enabling simulation of the STS motion, it does not include all DoFs that humans have. For instance, ankle eversion range of motion is known to significantly correlate with balance stability [49] but is not incorporated in the model. Additionally, user trust is not accounted for in the model. The omission of these aspects should be acknowledged as a simplification in the model.
- Specifically for the PM, it is important to keep in mind that by not modeling additional DoFs at the stump-socket interface, soft tissue artifacts are neglected. While this approach is common [28, 50, 51] and expected to have minimal influence [51], it more closely resembles an osseointegrated prosthesis rather than a socket prosthesis [30, 51].
- This study aimed to create a universal model for a highly personalized scenario: each amputation surgery varies, and every individual is unique. Since muscle tissues do not hold sutures well [25], the decision was made to assume that only the tendon was changed. However, in cases where the tendon cannot be preserved for myodesis, the muscle may be used instead [25], resulting in varied

muscle properties in the musculoskeletal model. Surgeons also differ in their methods of reattaching muscles and positioning the hip during muscle fixation [26], which can influence muscle properties. Due to significant variability in the literature regarding muscle strength in residual limbs [28], the maximum isometric force was kept unchanged, acknowledging the potential for overestimation of muscle forces [29, 30].

- Another limitation of the framework is the selection of muscles involved in the myodesis procedure: specifically, the RFEM and HAM for the PM. According to the studies reviewed by Fabre et al. [25], all 33 studies that performed myodesis included the ADDMAG muscle, while a smaller number (24 studies) additionally considered the quadriceps and/or hamstrings. It should be noted that not all of these studies incorporated these muscles for additional myodesis; some merely sutured them to or over the muscular complex. For the PM, only the RFEM and HAM were included, with the ADDMAG muscle left unchanged. This decision was influenced by the high attachment point of the ADDMAG in the musculoskeletal model, which remains unaffected by femur shortening. However, in reality, the ADDMAG is a large triangular muscle located on the medial side of the thigh, and its insertion is lost during transfemoral amputation, necessitating consideration [25].
- In both BM and PM, the thoracic movement is modeled with a single thoracic joint, confining upper body movement to the lumbar region and a single spinal position. While this constraint may not greatly affect the BM, given its limited thoracic movement prior to standing up, it could significantly impact the PM, which exhibits increased thorax extension. Integrating multiple thoracic joints would more accurately replicate human motion and could alter compensation strategies.
- While the goal of this study was to enable predictive simulations to uncover compensation strategies, measures were introduced to expedite simulation time. These measures guided the first few simulations toward realistic trajectories by limiting certain DoFs, such as hip adduction and pelvis tilt, to prevent unnatural positions. Additionally, they ensured that movements such as lumbar and thorax extension were appropriately used, rather than relying excessively on one of them alone. However, these imposed constraints could potentially restrict movement in predetermined directions, potentially overlooking some compensation strategies.
- Lastly, an additional limitation of the optimization framework is the necessity to specify the standing-up time. In the simulation, this motion occurs as the pelvis has to reach a predefined height at 1.5 [s]. While this setting is essential for initiating the movement, it may partially contribute to the prolonged duration of phase P1 in the PM, as remaining seated for as long as possible minimizes muscle exertion. Consequently, caution should be exercised when interpreting differences in duration.

## V. Conclusion

A three-dimensional predictive simulation model has been developed for both non-amputees (baseline model) and unilateral transfemoral amputees. This framework facilitates the optimization of ankle and knee stiffness and damping prosthesis parameters. Such optimization presents an opportunity to customize prostheses specifically for the sit-to-stand movement in the future, potentially minimizing secondary prosthesis-related health conditions associated with one of the most mechanically demanding tasks of daily life: standing-up.


## Acknowledgments

This study was conducted as a Master's Thesis project to fulfill the requirements for the Master's degree in Mechanical Engineering, focusing specifically on the Biomechanical Design track. The results of this study would not have been achieved without the invaluable assistance of my supervisors, Eline van der Kruk and Bob van der Windt. I am grateful to Bob for his flexibility, regular meetings, and brainstorming sessions regarding result interpretation, as well as his assistance whenever I encountered challenges. I would also like to express my thanks to Eline for her expertise and enthusiasm for this project. Additionally, I extend my appreciation to Thomas Geijtenbeek for providing the Hyfydy licenses and for promptly responding to my questions. Another thank you to Reslin Schelhaas, PhD candidate at UMCG, who kindly discussed her research on how amputation surgeons choose their methods and helped me understand current methods in more depth. Finally, I would like to thank Mads Christensen for our discussions on overcoming specific challenges and for sharing his MATLAB set for muscle activation, which we hope to incorporate in future work.


## Data Availability

The data used to generate the results shown in this study, as well as the generated videos, are available in the following GitHub repository: https://github.com/karinvanminnen/STSprosthesis.

## REFERENCES


[1] M. Marino, S. Pattni, M. Greenberg, A. Miller, E. Hocker, S. Ritter, and K. Mehta, "Access to prosthetic devices in developing countries: Pathways and challenges," *Proceedings of the 5th IEEE Global Humanitarian Technology Conference, GHTC 2015*, pp. 45–51, 12 2015.

[2] M. Windrich, M. Grimmer, O. Christ, S. Rinderknecht, and P. Beckerle, "Active lower limb prosthetics: a systematic review of design issues and solutions," *BioMedical Engineering OnLine*, vol. 15, no. Suppl 3, 12 2016. [Online]. Available: /pmc/articles/PMC5249019//pmc/articles/PMC5249019/?report=abstracthttps://www.ncbi.nlm.nih.gov/pmc/articles/PMC5249019/

[3] K. Mordarska and M. Godziejewska-Zawada, "Diabetes in the elderly," *Przeglad Menopauzalny = Menopause Review*, vol. 16, no. 2, pp. 38–43, 2017. [Online]. Available: /pmc/articles/PMC5509969//pmc/articles/PMC5509969/?report=abstracthttps://www.ncbi.nlm.nih.gov/pmc/articles/PMC5509969/

[4] A. S. D. M. Matheus, L. R. M. Tannus, R. A. Cobas, C. C. Palma, C. A. Negrato, and M. D. B. Gomes, "Impact of diabetes on cardiovascular disease: An update," *International Journal of Hypertension*, vol. 2013, 2013.

[5] W. H. Van Houtum, L. A. Lavery, and L. B. Harkless, "The impact of diabetes-related lower-extremity amputations in the Netherlands," *Journal of Diabetes and its Complications*, vol. 10, no. 6, pp. 325–330, 11 1996.

[6] International Diabetes Federation, "Diabetes Complications," 2024. [Online]. Available: https://idf.org/about-diabetes/diabetes-complications/

[7] H. Burger and Ä. Marinček, "The life style of young persons after lower limb amputation caused by injury," *Prosthetics and orthotics international*, vol. 21, no. 1, pp. 35–39, 1997. [Online]. Available: https://pubmed.ncbi.nlm.nih.gov/9141124/

[8] I. Kovac, K. Neven, Å. Ognjen, M. Vedrana, A. Marina, V. Zoran, V. Tamara, N. Istvanović, and L. Branko, "Rehabilitation of lower limb amputees," *Periodicum Biologorum*, vol. 117, pp. 147–159, 2 2015.

[9] S. Demirdel and Ä. Ülger, "Body image disturbance, psychosocial adjustment and quality of life in adolescents with amputation," *Disability and health journal*, vol. 14, no. 3, 7 2021. [Online]. Available: https://pubmed.ncbi.nlm.nih.gov/33589407/

[10] A. S. Göktepe, B. Cakir, B. Yilmaz, and K. Yazicioglu, "Energy expenditure of walking with prostheses: Comparison of three amputation levels," *Prosthetics and Orthotics International*, vol. 34, no. 1, pp. 31–36, 3 2010.

[11] R. Gailey, K. Allen, J. Castles, J. Kucharik, and M. Roeder, "Review of secondary physical conditions associated with lower-limb amputation and long-term prosthesis use," pp. 15–30, 2008.

[12] P. M. Dall and A. Kerr, "Frequency of the sit to stand task: An observational study of free-living adults," *Applied Ergonomics*, vol. 41, no. 1, pp. 58–61, 2010.

[13] P. O. Riley, M. L. Schenkman, R. W. Mann, and W. A. Hodge, "Mechanics of a constrained chair-rise," *Journal of Biomechanics*, vol. 24, no. 1, pp. 77–85, 1 1991.

[14] H. A. Varol, F. Sup, and M. Goldfarb, "Powered sit-to-stand and assistive stand-to-sit framework for a powered transfemoral prosthesis," in *2009 IEEE International Conference on Rehabilitation Robotics, ICORR 2009*, 2009, pp. 645–651.

[15] C. R. Claret, G. W. Herget, L. Kouba, D. Wiest, J. Adler, V. Von Tscharner, T. Stieglitz, and C. Pasluosta, "Neuromuscular adaptations and sensorimotor integration following a unilateral transfemoral amputation," *Journal of NeuroEngineering and Rehabilitation*, vol. 16, no. 1, 9 2019. [Online]. Available: /pmc/articles/PMC6744715//pmc/articles/PMC6744715/?report=abstracthttps://www.ncbi.nlm.nih.gov/pmc/articles/PMC6744715/

[16] H. Charkhkar, B. P. Christie, and R. J. Triolo, "Sensory neuroprosthesis improves postural stability during Sensory Organization Test in lower-limb amputees," *Scientific Reports*, vol. 10, no. 1, 12 2020. [Online]. Available: /pmc/articles/PMC7181811//pmc/articles/PMC7181811/?report=abstracthttps://www.ncbi.nlm.nih.gov/pmc/articles/PMC7181811/

[17] M. J. Highsmith, J. T. Kahle, S. L. Carey, D. J. Lura, R. V. Dubey, K. R. Csavina, and W. S. Quillen, "Kinetic asymmetry in transfemoral amputees while performing sit to stand and stand to sit movements," *Gait and Posture*, vol. 34, no. 1, pp. 86–91, 5 2011.

[18] E. van der Kruk and T. Geijtenbeek, "A planar neuromuscular controller to simulate compensation strategies in the sit-to-walk movement," *PLOS ONE*, vol. 19, no. 6, p. e0305328, 6 2024. [Online]. Available: https://journals.plos.org/plosone/article?id=10.1371/journal.pone.0305328

[19] H. Geyer and H. Herr, "A muscle-reflex model that encodes principles of legged mechanics produces human walking dynamics and muscle activities," *IEEE transactions on neural systems and rehabilitation engineering : a publication of the IEEE Engineering in Medicine and Biology Society*, vol. 18, no. 3, pp. 263–273, 6 2010. [Online]. Available: https://pubmed.ncbi.nlm.nih.gov/20378480/

[20] E. van der Kruk, P. Strutton, L. J. Koizia, M. Fertleman, P. Reilly, and A. M. J. Bull, "Why do older adults stand-up differently to young adults?: investigation of compensatory movement strategies in sit-to-walk," *npj Aging*, vol. 8, no. 1, 9 2022.

[21] J. M. Wang, S. R. Hamner, S. L. Delp, and V. Koltun, "Optimizing Locomotion Controllers Using Biologically-Based Actuators and Objectives," *ACM transactions on graphics*, vol. 31, no. 4, 7 2012. [Online]. Available: https://pubmed.ncbi.nlm.nih.gov/26251560/

[22] T. Geijtenbeek, "SCONE: Open Source Software for Predictive Simulation of Biological Motion," *Journal of Open Source Software*, vol. 4, no. 38, p. 1421, 6 2019. [Online]. Available: https: //joss.theoj.org/papers/10.21105/joss.01421

[23] T. Geijtenbeek, "The Hyfydy Simulation Software," 11 2021. [Online]. Available: https://hyfydy.com

[24] V. Raveendranathan and R. Carloni, "Musculoskeletal Model of an Osseointegrated Transfemoral Amputee in OpenSim," *Proceedings of the IEEE RAS and EMBS International Conference on Biomedical Robotics and Biomechatronics*, vol. 2020-November, pp. 1196–1201, 11 2020.

[25] I. Fabre, D. Thompson, B. Gwilym, K. Jones, M. Pinzur, J. H. Geertzen, C. Twine, and D. Bosanquet, "Surgical Techniques of, and Outcomes after, Distal Muscle Stabilization in Transfemoral Amputation: A Systematic Review and Narrative Synthesis," *Annals of vascular surgery*, vol. 98, pp. 182–193, 1 2024. [Online]. Available: https://pubmed.ncbi.nlm.nih.gov/37802139/

[26] R. Schelhaas, K. van Kammen, R. Dekker, H. Houdijk, J.-P. P. de Vries, P. C. Jutte, and J. H. Geertzen, "Concept final proof - Technique Selection in Transfemoral Amputation Surgery," *Medical Research Archives*, vol. 12, no. 7, 2024.

[27] D. G. Smith, "Surgery and Postoperative Care Surgery," *Amputee Coalition*, vol. 14, no. 3, 5 2004.

[28] A. M. Willson, A. J. Anderson, C. A. Richburg, B. C. Muir, J. Czerniecki, K. M. Steele, and P. M. Aubin, "Full body musculoskeletal model for simulations of gait in persons with transtibial amputation," *Computer Methods in Biomechanics and Biomedical Engineering*, vol. 26, no. 4, pp. 412–423, 2023.

[29] V. Harandi, D. Ackland, R. Haddara, L. Lizama, M. Graf, M. Galea, and P. Lee, "Gait compensatory mechanisms in unilateral transfemoral amputees," *Medical Engineering and Physics*, vol. 77, pp. 95–106, 2020.

[30] N. W. Vandenberg, J. W. Stoneback, H. Davis-Wilson, C. L. Christiansen, M. E. Awad, D. H. Melton, and B. M. Gaffney, "Unilateral transfemoral osseointegrated prostheses improve joint loading during walking," *Journal of Biomechanics*, vol. 155, 6 2023.

[31] S. L. Delp, J. P. Loan, M. G. Hoy, F. E. Zajac, E. L. Topp, and J. M. Rosen, "An Interactive Graphics-Based Model of the Lower Extremity to Study Orthopaedic Surgical Procedures," *IEEE Transactions on Biomedical Engineering*, vol. 37, no. 8, pp. 757–767, 1990.

[32] A. Rajagopal, C. L. Dembia, M. S. DeMers, D. D. Delp, J. L. Hicks, and S. L. Delp, "Full-Body Musculoskeletal Model for Muscle-Driven Simulation of Human Gait," *IEEE transactions on bio-medical engineering*, vol. 63, no. 10, pp. 2068–2079, 10 2016. [Online]. Available: https://pubmed.ncbi.nlm.nih.gov/27392337/

[33] A. D. Walkowski and S. Munakomi, "Monosynaptic Reflex," *StatPearls*, 9 2022. [Online]. Available: https://www.ncbi.nlm.nih.gov/books/NBK541028/

[34] H. S. Friedman and C. E. Priebe, "Estimating stimulus response latency," *Journal of Neuroscience Methods*, vol. 83, no. 2, pp. 185–194, 9 1998.

[35] I. L. Kurtzer, "Long-latency reflexes account for limb biomechanics through several supraspinal pathways," *Frontiers in Integrative Neuroscience*, vol. 8, no. JAN, 1 2014. [Online]. Avail-able: /pmc/articles/PMC4310276//pmc/articles/PMC4310276/?report= abstracthttps://www.ncbi.nlm.nih.gov/pmc/articles/PMC4310276/

[36] E. Caruthers, J. Kolesar, A. Chaudhari, L. Schmitt, T. Best, K. Saul, and R. Siston, "Muscle Forces and Their Contributions to Vertical and Horizontal Acceleration of the Center of Mass During Sit-to-Stand Transfer in Young, Healthy Adults," *Journal of Applied Biomechanics*, vol. 32, 4 2016.

[37] "Power Knee." [Online]. Available: https://www.ossur.com/en-us/prosthetics/knees/power-knee

[38] "C-Leg 4 — Kies voor nieuwe, bewezen prestaties." [Online]. Available: https://www.ottobock.com/nl-nl/product/3C88-3~23C98-3

[39] "Mauch® Knee." [Online]. Available: https://www.ossur.com/nl-nl/prosthetics/knieen/mauch-knee

[40] J. M. Kim, H. D. Je, and H. D. Kim, "Effects of pelvic compression belts on the kinematics and kinetics of the lower extremities during sit-to-stand maneuvers," *Journal of Physical Therapy Science*, vol. 29, no. 8, pp. 1311–1317, 2017. [Online]. Available: https://www.researchgate.net/publication/318999180_Effects_of_pelvic_compression_belts_on_the_kinematics_and_kinetics_of_the_lower_extremities_during_sit-to-stand_maneuvers
[41] H. Wang, S. Xu, J. Fu, X. Xu, Z. Wang, and R. S. Na, "Sit-to-Stand (STS) Movement Analysis of the Center of Gravity for Human-Robot Interaction," *Frontiers in Neurorobotics*, vol. 16, p. 863722, 5 2022.
[42] E. J. Rouse, R. D. Gregg, L. J. Hargrove, and J. W. Sensinger, "The difference between stiffness and quasi-stiffness in the context of biomechanical modeling," *IEEE transactions on bio-medical engineering*, vol. 60, no. 2, pp. 562–568, 2013. [Online]. Available: https://pubmed.ncbi.nlm.nih.gov/23212310/
[43] M. Wu, M. R. Haque, and X. Shen, "Obtaining Natural Sit-to-Stand Motion with a Biomimetic Controller for Powered Knee Prostheses," *Journal of Healthcare Engineering*, vol. 2017, 2017.
[44] S. L. Hoffman, M. B. Johnson, D. Zou, and L. R. Van Dillen, "Differences in end-range lumbar flexion during slumped sitting and forward bending between low back pain subgroups and genders," *Manual Therapy*, vol. 17, no. 2, p. 157, 4 2012. [Online]. Available: /pmc/articles/PMC3288514//pmc/articles/PMC3288514/?report=abstracthttps://www.ncbi.nlm.nih.gov/pmc/articles/PMC3288514/
[45] H. Burger, J. Kuželički, and Ä. R. Marinek, "Transition from sitting to standing after trans-femoral amputation," *Prosthetics and Orthotics International*, vol. 29, no. 2, pp. 139–151, 8 2005.
[46] G. Valle, A. Saliji, E. Fogle, A. Cimolato, F. M. Petrini, and S. Raspopovic, "Mechanisms of neuro-robotic prosthesis operation in leg amputees," *Science Advances*, vol. 7, no. 17, pp. 8354–8375, 4 2021. [Online]. Available: /pmc/articles/PMC8059925//pmc/articles/PMC8059925/?report=abstracthttps://www.ncbi.nlm.nih.gov/pmc/articles/PMC8059925/
[47] G. Klute, C. Kallfelz, and J. Czerniecki, "Mechanical properties of prosthetic limbs: Adapting to the patient," *Journal of rehabilitation research and development*, vol. 38, pp. 299–307, 8 2001.
[48] O. N. Beck, P. Taboga, and A. M. Grabowski, "Characterizing the Mechanical Properties of Running-Specific Prostheses," *PLoS ONE*, vol. 11, no. 12, 12 2016. [Online]. Available: /pmc/articles/PMC5156386//pmc/articles/PMC5156386/?report=abstracthttps://www.ncbi.nlm.nih.gov/pmc/articles/PMC5156386/
[49] S. K. Bok, T. H. Lee, and S. S. Lee, "The Effects of Changes of Ankle Strength and Range of Motion According to Aging on Balance," *Annals of Rehabilitation Medicine*, vol. 37, no. 1, p. 10, 2013. [Online]. Available: /pmc/articles/PMC3604218//pmc/articles/PMC3604218/?report=abstracthttps://www.ncbi.nlm.nih.gov/pmc/articles/PMC3604218/
[50] T. Templin, G. Klute, and R. Neptune, "The Influence of Load Carriage on Knee Joint Loading and Metabolic Cost on Walking with Lower-Limb Amputation: A Preliminary Modeling Study," *Journal of Prosthetics and Orthotics*, vol. 33, no. 2, pp. 118–124, 2021.
[51] B. M. Gaffney, N. W. Vandenberg, H. C. Davis-Wilson, C. L. Christiansen, G. F. Roda, G. Schneider, T. Johnson, and J. W. Stoneback, "Biomechanical compensations during a stand-to-sit maneuver using transfemoral osseointegrated prostheses: A case series," *Clinical Biomechanics*, vol. 98, 8 2022.
[52] L. Paterno, M. Filosa, E. Anselmino, A. Cecere, F. Dell'agnello, E. Gruppioni, A. Mazzoni, S. Micera, C. Oddo, and A. Menciassi, "Soft Transfemoral Prosthetic Socket With Sensing and Augmenting Feedback: A Case Study," *IEEE Transactions on Medical Robotics and Bionics*, vol. 6, no. 2, pp. 536–547, 5 2024. [Online]. Available: https://www.researchgate.net/publication/379365084_Soft_Transfemoral_Prosthetic_Socket_With_Sensing_and_Augmenting_Feedback_A_Case_Study
[53] Össur, "RHEO KNEE Microprocessor Knee — Prosthetic Knee — Ossur.com." [Online]. Available: https://www.ossur.com/en-us/prosthetics/knees/rheo-knee#specificationContentAnchor
[54] PROTEOR, "Highlander and Highlander MAX - Proteor USA." [Online]. Available: https://us.proteor.com/feet/highlander/#flush-heading-block_3181d269e555849acf219cf8967f1bf6-0
[55] Össur, "Prosthetic Feet. Ossur.com." [Online]. Available: https://www.ossur.com/en-us/prosthetics/products/feet
[56] Bone & Joint Clinic, "Prosthetics and Orthotics," 2024. [Online]. Available: https://boneandjointclinic.com/405-2/

# APPENDIX

## A. Muscle-Tendon Shortening

The properties of the reattached RFEM and HAM are based on their decrease in total size due to the new insertion points. This amount of decrease is then subtracted from the original tendon slack length, resulting in the values of Table I. For the RFEM, the mean difference between hip flexion and muscle-tendon length was 0.1306 [m], while for the HAM, this value was 0.2034 [m] (Figure A.1).

## B. Mass and Inertia Calculations

Creating an accurate Hyfydy model for an individual with a transfemoral prosthesis involves adjusting the mass and inertia properties to reflect the presence of the prosthesis. The Hyfydy model used a combined file for the residual femur and the upper leg part of the prosthesis. Underneath the estimations for the combined residual femur and upper leg part of the prosthesis, the prosthetic lower leg part, and the prosthetic foot are described. These estimations are based on general prosthetic component weights and properties.

*1) Residual Femur & Upper Leg Prosthesis:* Since the femur is amputated, its mass and inertia properties are approximated by halving the original femur properties. The original femur has the following mass and inertia properties:

$$\text{Mass} : 9.3014\,[\text{kg}]$$
$$\text{Inertia} : \begin{cases} x = 0.1339 \\ y = 0.0351 \\ z = 0.1412 \end{cases} \quad [\text{kg}{\cdot}\text{m}^2]$$

The new residual femur is adapted to the following properties:

$$\text{Mass} : 4.6507\,[\text{kg}]$$
$$\text{Inertia} : \begin{cases} x = 0.06695 \\ y = 0.01755 \\ z = 0.0706 \end{cases} \quad [\text{kg}{\cdot}\text{m}^2]$$

For the upper leg part of the prosthesis: A typical transfemoral prosthetic upper leg part (including the socket) weighs approximately 1-2 [kg] (for example, the augmented socket of Paterno et al. [52] weighs 1.8 [kg]). Therefore, for the upper leg part of the prosthesis an average prosthetic upper leg weight of 1.5 [kg] is assumed. Inertia properties for the prosthetic upper leg can be simplified as being proportional to its mass and distributed along similar axes as the biological limb.

Combining the residual femur and prosthetic upper leg part, results in the following properties:

$$\begin{aligned} \text{Total mass} : {} & 4.6507\,[\text{kg}]\ \text{(residual femur)} \\ & + 1.5\,[\text{kg}]\ \text{(prosthetic upper leg and socket)} \\ & = 6.1507\,[\text{kg}] \end{aligned}$$

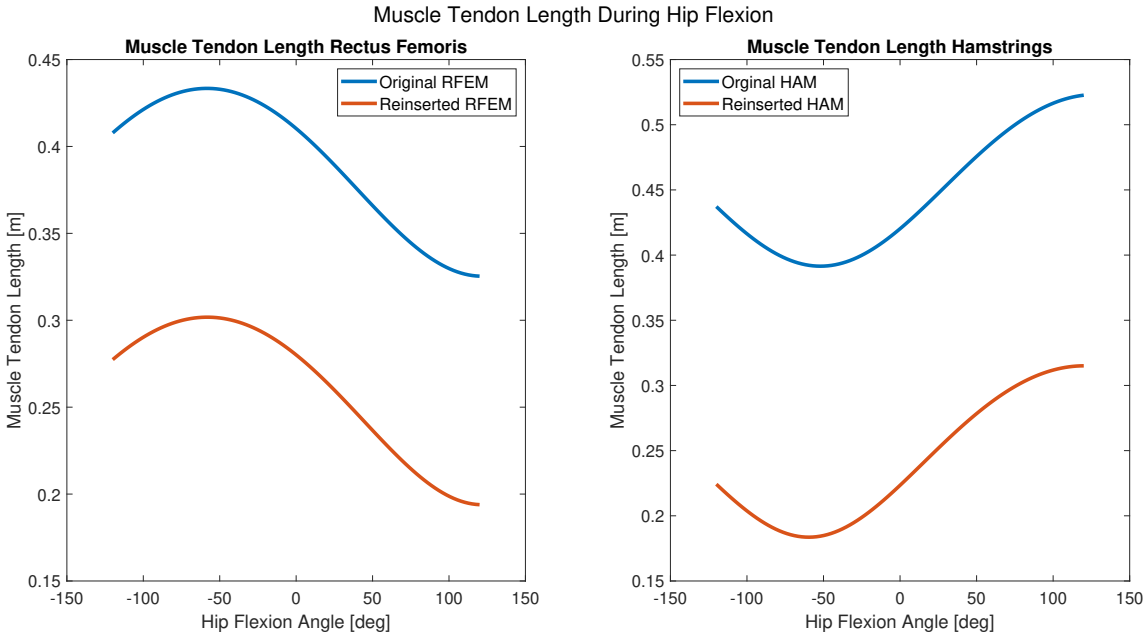


Fig. A.1: Change in MTU length during hip flexion for reattached and original muscles, based on data for RFEM and Biceps Femoris Long Head from Raveendranathan and Carloni [24]. The mean difference is used to adjust the tendon slack length of the reattached muscles.

$$\text{Inertia} : \begin{cases} x \approx 0.08034 \\ y \approx 0.02106 \\ z \approx 0.08472 \end{cases} \quad [\text{kg}\cdot\text{m}^2]$$

*2) Prosthetic Lower Leg:* A typical prosthetic lower leg (tibia) weighs around 1-2 [kg] (such as the RHEO Microprocessor knee [53] that is 1.6 [kg]). An average value of 1.5 [kg] is therefore assumed. For the inertia properties, the biological tibia is proportionally scaled down to the mass difference. The tibia's inertia is scaled by the ratio of the prosthetic mass to the biological mass ($\frac{1.5}{3.7075} \approx 0.405$).

The original tibia has the following inertia:

$$\text{Inertia} : \begin{cases} x = 0.0504 \\ y = 0.0051 \\ z = 0.0511 \end{cases} \quad [\text{kg}\cdot\text{m}^2]$$

The new prosthetic lower leg is adapted to the following properties:

$$\text{Inertia} : \begin{cases} x \approx 0.02042 \\ y \approx 0.00207 \\ z \approx 0.02068 \end{cases} \quad [\text{kg}\cdot\text{m}^2]$$

*3) Prosthetic Foot:* A prosthetic foot generally weighs around 0.5-1 [kg], as exemplified by those from PROTEOR [54] and Össur [55]. A weight of 0.75 [kg] is assumed.

$$\text{Mass} : 0.75\,[\text{kg}]$$

For the inertia properties, the biological calcaneus is scaled down proportionally to the mass difference ($\frac{0.75}{1.25} = 0.6$).

The original calcaneus has the following inertia:

$$\text{Inertia} : \begin{cases} x = 0.0014 \\ y = 0.0039 \\ z = 0.0041 \end{cases} \quad [\text{kg}\cdot\text{m}^2]$$

The new prosthetic foot is adapted to the following properties:

$$\text{Inertia} : \begin{cases} x \approx 0.00084 \\ y \approx 0.00234 \\ z \approx 0.00246 \end{cases} \quad [\text{kg}\cdot\text{m}^2]$$

All values are summarized in Table II. Using these values, the total modeled prosthetic leg weighs 3.75 [kg] (1.5 + 1.5 + 0.75 [kg]), which is consistent with Bone & Joint Clinic [56], who state that a typical transfemoral prosthesis weighs 8 [lbs], approximately 3.63 [kg].

### C. Muscle Activation & Force

*1) Muscle Activation Baseline Model versus Caruthers et al.:* While numerical comparison between the experimental and simulated muscle activations of Caruthers et al. [36] and the BM is challenging due to a lack of exact numbers, shape comparisons can be made using the graphs in Figure A.2. This indicates that while the GMAX reaches a higher activation in the BM, the shape remains similar. In contrast, the GMED and SOL in the BM show a more pronounced peak than in the data of Caruthers et al. [36], whereas the RFEM exhibits a lower activation pattern. The VAS shows a similar trend, as do the TA, GAS (compared with the medial gastrocnemius), and HAM (compared with the biceps femoris long head).

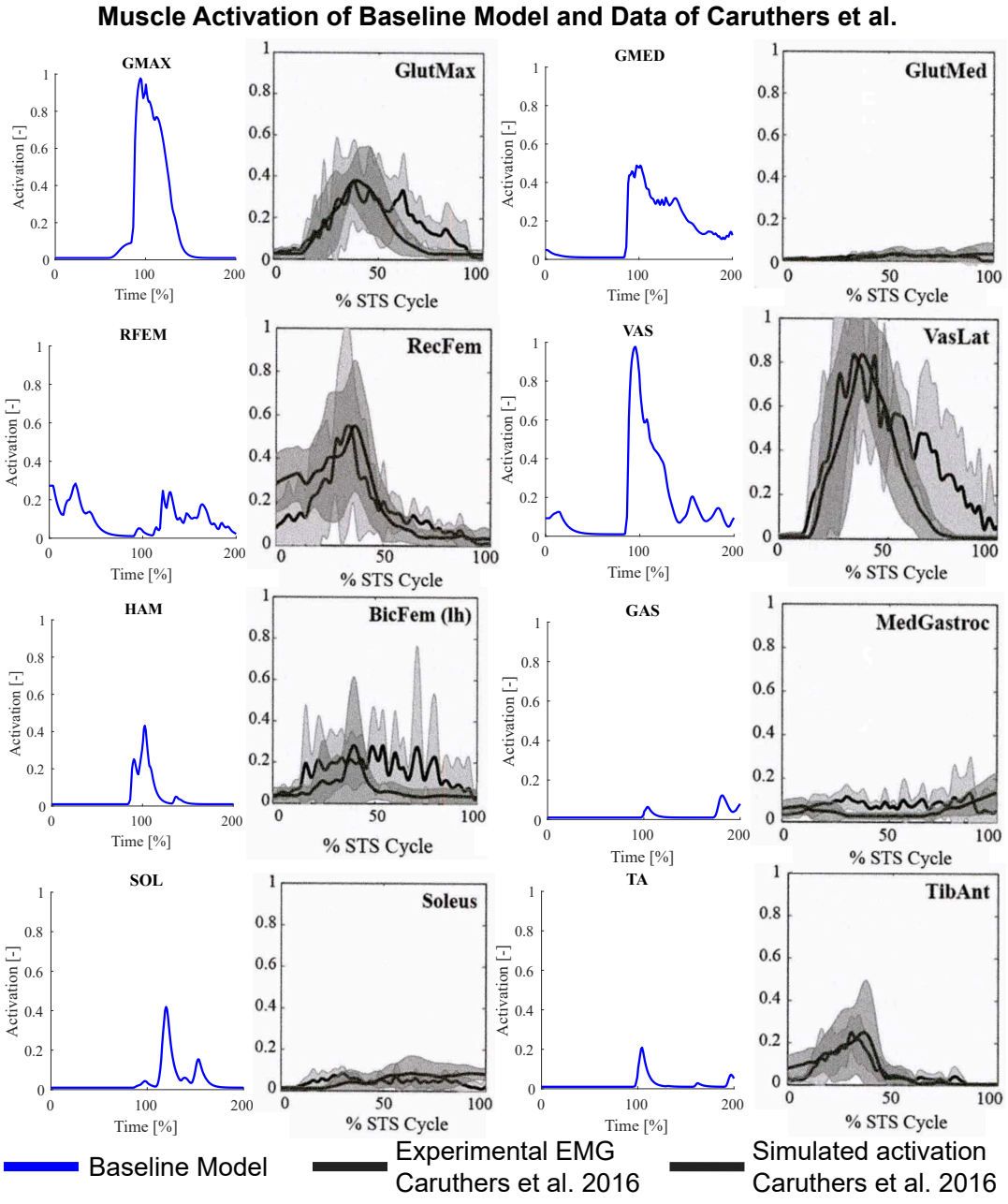


Fig. A.2: Comparison of muscle activation between the mean of both legs of BM and experimental and simulation activation of Caruthers et al. [36], with the shaded area indicating one standard deviation.

*2) Muscle Activation Baseline Model versus Prosthesis Model:* Figure A.3 compares the muscle activations of the BM with the PM, indicating that PM requires higher muscle activation, even for balancing, compared to BM.

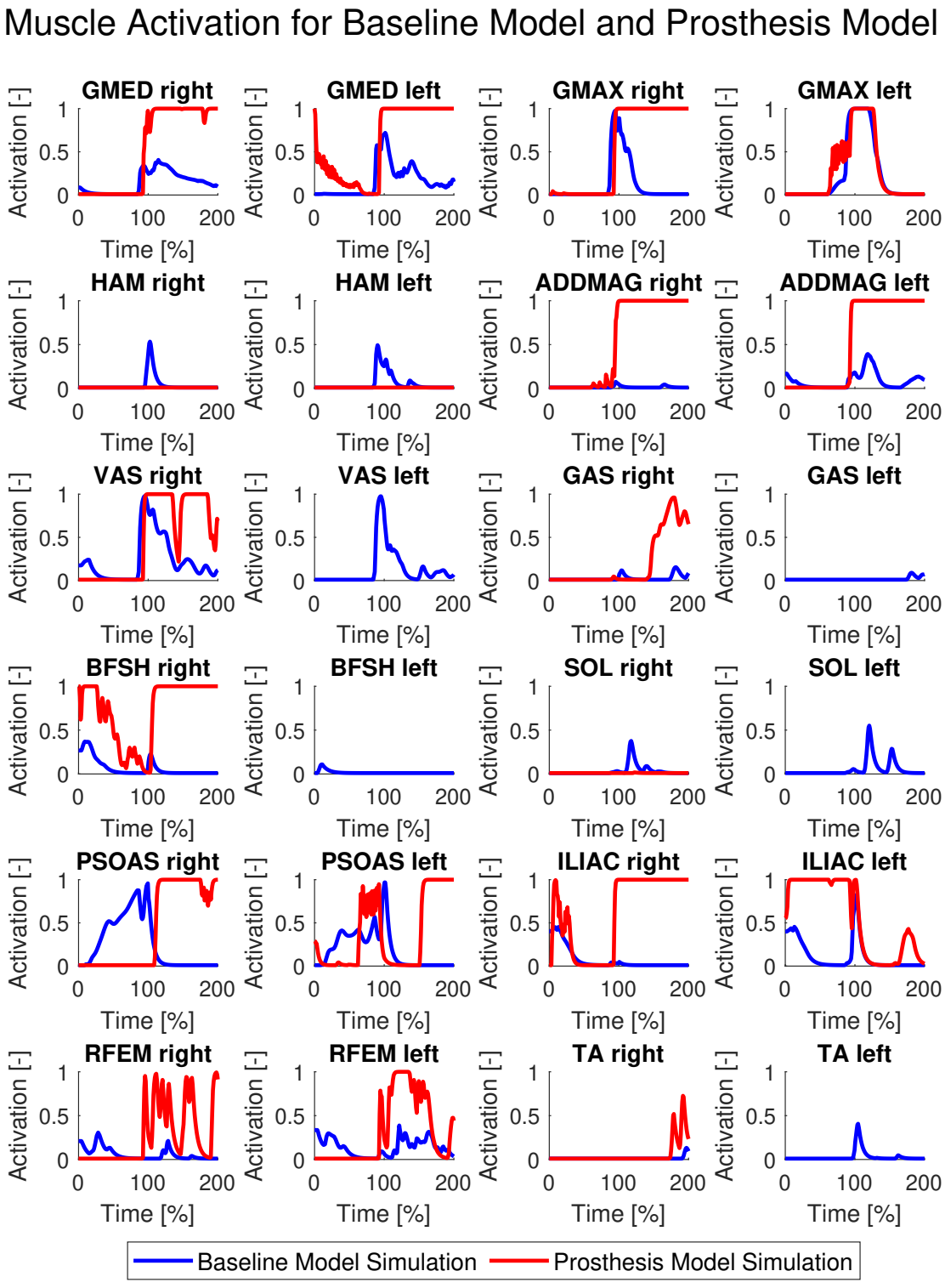


Fig. A.3: Muscle activation during the normalized STS motion for BM and PM. Note that in the PM, the left leg represents the prosthetic leg.

*3) Muscle Force Baseline Model versus Prosthesis Model and Experimental Data:* Figure A.4 compares the muscle forces of the BM and PM, as well as the muscle forces calculated using the model by van der Kruk et al. [20], which is based on experimental data. The figure illustrates that the PM consistently requires similar or higher muscle forces compared to the BM, except for the right HAM and right SOL.

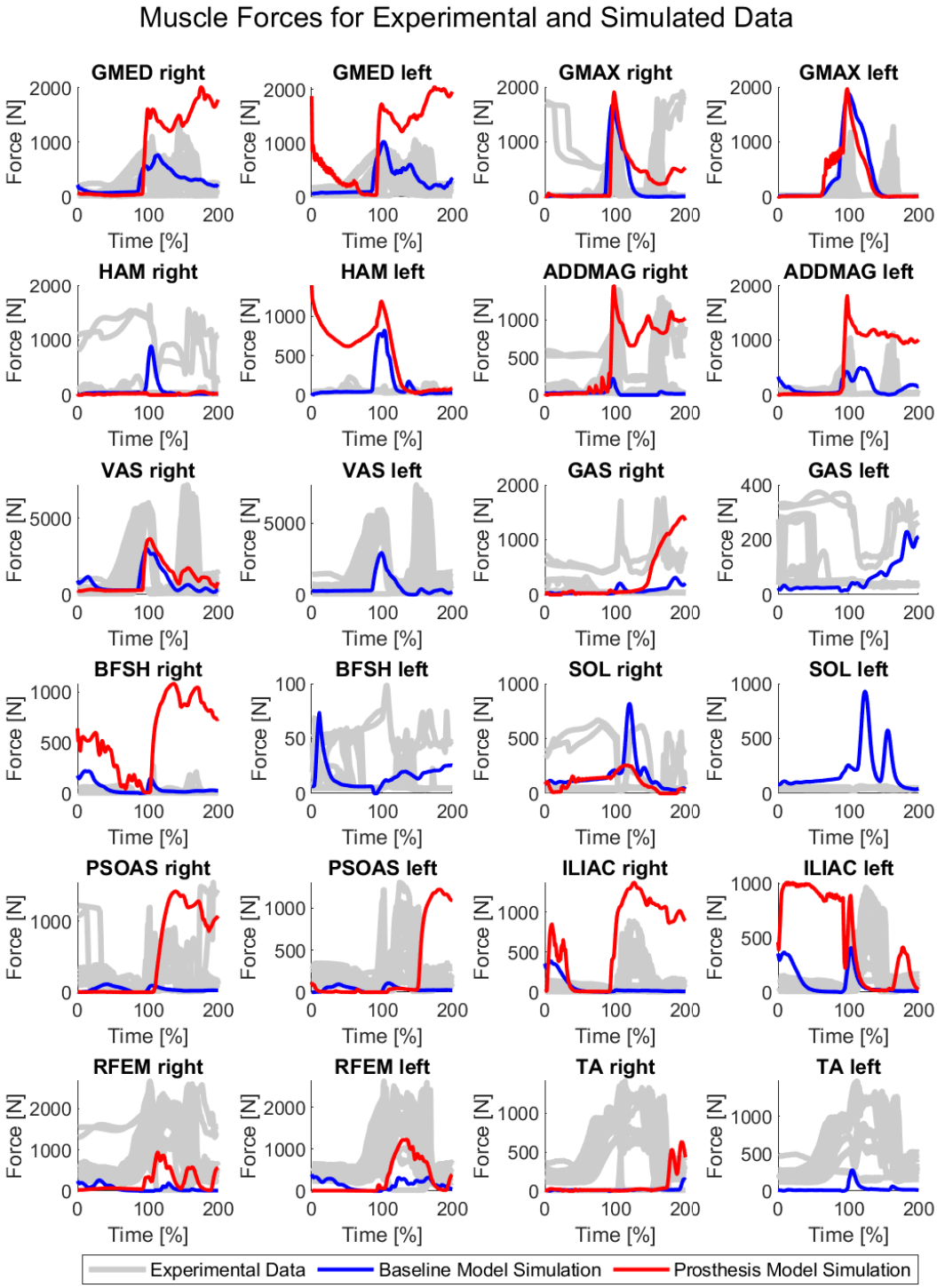


Fig. A.4: Muscles forces for BM and PM with each experimental trial of van der Kruk et al. [20] displayed in grey.

### D. Experimental Joint Angles

Figure A.5 presents the individual joint angles from all experimental trials for all participants, highlighting the differences between the experiments.

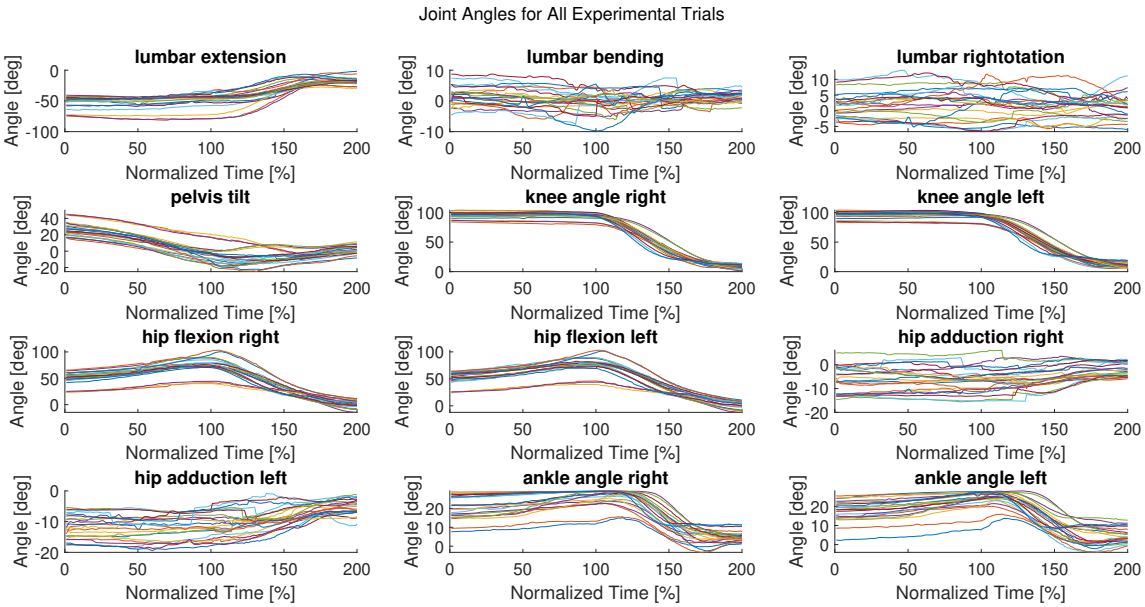


Fig. A.5: Experimental joint angles for all trials of all participants, normalized over time before seat off (at 100%) and after seat off.

### E. Ground Reaction Force over Time

Figure A.6 illustrates how the GRF of both legs changes over time for the BM and PM. It indicates that, although both legs contribute to the standing-up motion of the PM, there is a discrepancy in the amount of force they exert on the ground as time progresses.

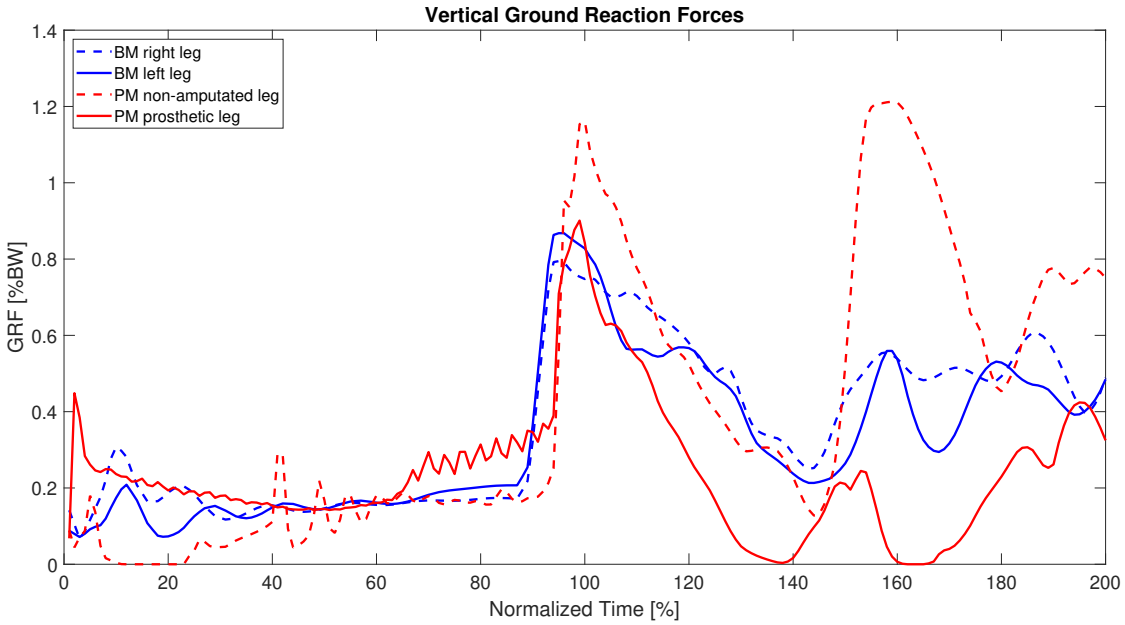


Fig. A.6: Vertical GRF over normalized time for both the BM and PM.

### *F. Hamstring Muscle Properties*

The decision to change only the tendon slack length of the reinserted HAM and RFEM resulted in the HAM muscle not being activated (Figure A.3), despite producing a force that is more than half of its maximum isometric force (Figure 9). Therefore, it appears that merely changing the tendon slack length may not be effective, as it seems to produce only passive forces. An attempt was made to investigate the outcomes by also altering the optimal fiber length. The results of Figure A.7 are achieved with an optimal fiber length of 0.075 [m] (originally 0.0976 [m]), while the tendon slack length is 0.18 [m] (originally 0.3250 [m], and 0.1216 [m] in the musculoskeletal models used in this paper). This illustrates that achieving more realistic activations for the HAM is possible. However, further research is required to develop an accurate method for adjusting its properties.

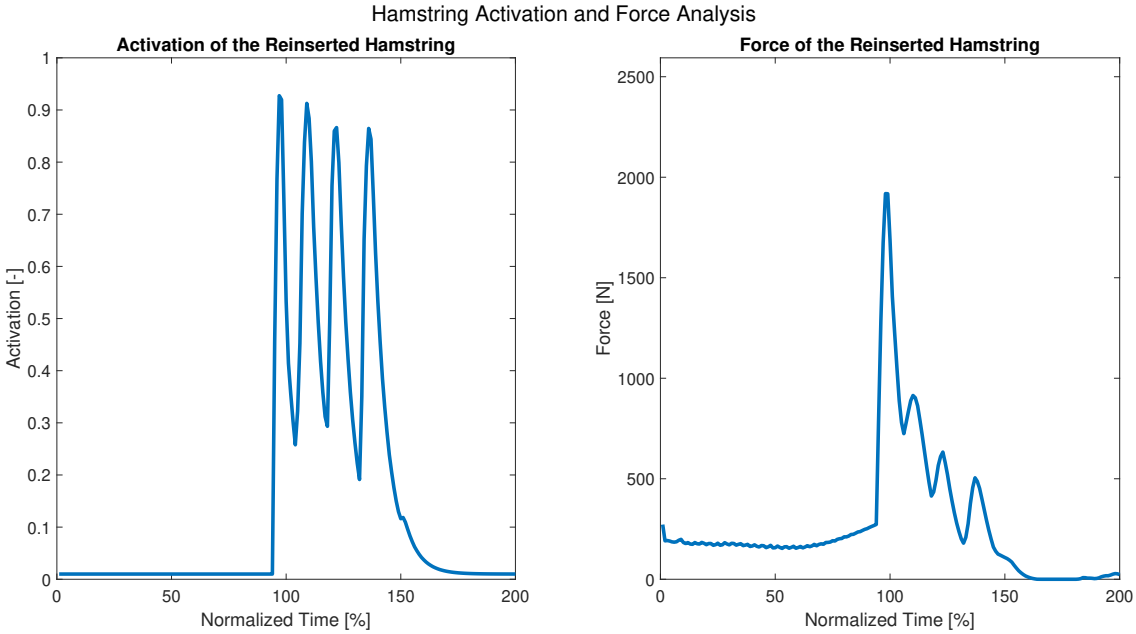


Fig. A.7: Activation and force of the reinserted HAM in case the tendon slack length is set to 0.18 [m] and the optimal fiber length is changed to 0.075 [m]

## G. MATLAB analysis

Figure A.8 illustrates the setup of the MATLAB framework, showing various functions for extracting information or calculating values. Each of the files contains comments providing additional explanations.

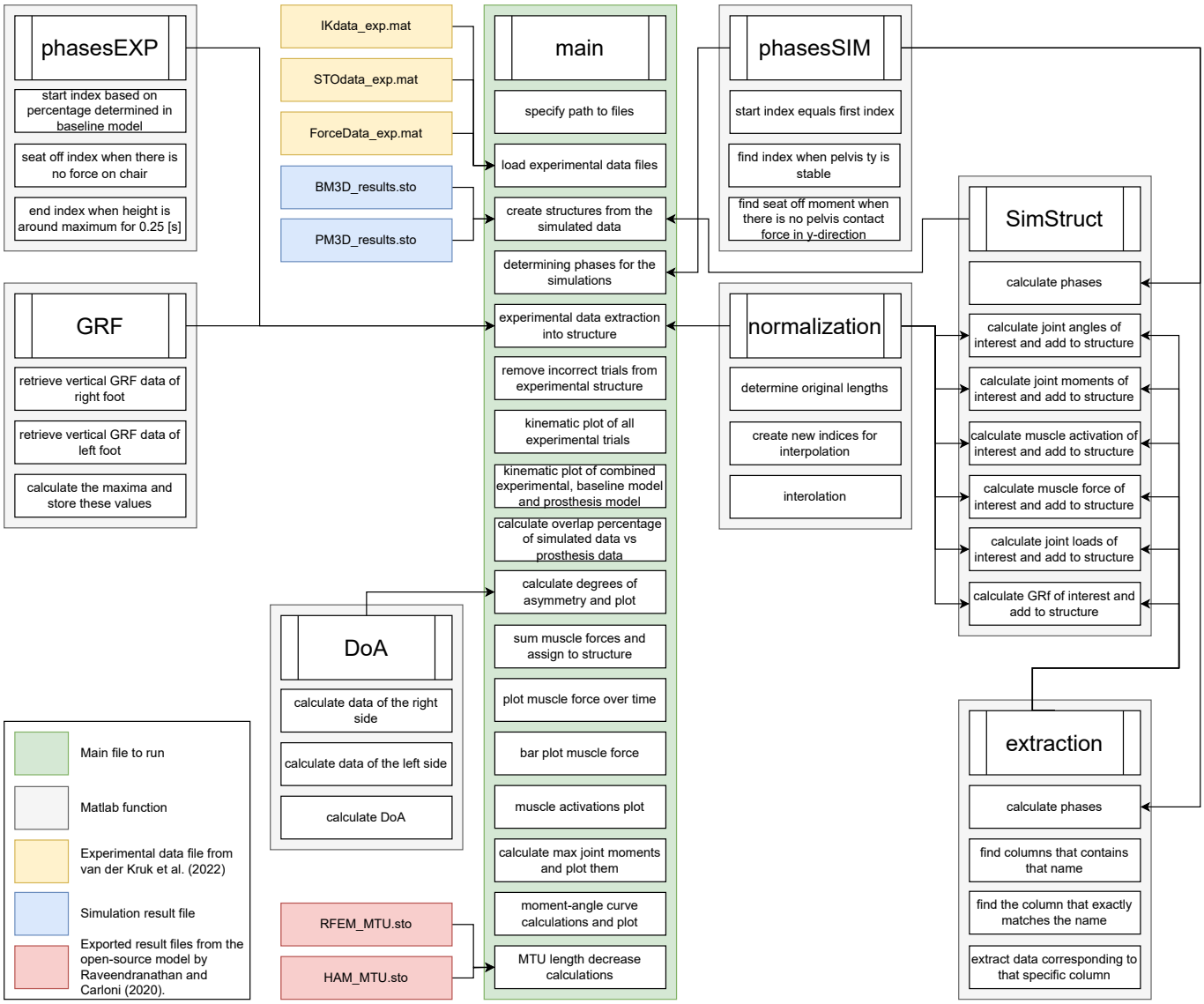


Fig. A.8: Overview of the MATLAB framework used for all the data analysis.

### H. ScriptMeasure

To ensure the PM uses both legs during standing up and avoids converging to undesired local minima, a ScriptMeasure was implemented. A ScriptMeasure is defined by a Lua script [22]. Within the SCONE file, the ScriptMeasure was incorporated by specifying the target body, the prosthetic foot, indicating that the measure should be minimized, and defining the path to the Lua file. The Lua file, as shown in Code 1, identifies the specified body from the SCONE file, retrieves its vertical position, computes its displacement over subsequent stages, and returns this value. This displacement is then minimized. The code snippet provided calculates vertical foot displacement, and a similar approach is applied to control horizontal displacement to prevent forward stepping.

```lua
function init( model, par, side )
    -- get the 'target_body' parameter from ScriptMeasure
    target_body = scone.target_body

    -- find the actual body with the same name
    body = model:find_body( target_body )

    -- initialize displacement integral
    foot_displacement = 0

    -- store initial foot position
    initial_foot_pos = body:com_pos().y
end

function update( model )
    -- get current vertical position of the foot
    local current_foot_pos = body:com_pos().y

    -- compute the displacement from the initial position
    local displacement = math.abs(current_foot_pos - initial_foot_pos)

    -- update the displacement integral
    foot_displacement = foot_displacement + model:delta_time() * displacement
end

function result(model)
    -- this is called at the end of the simulation
    -- fitness corresponds to the minimized foot displacement
    local fitness = foot_displacement / model:max_duration()

    return fitness
end

function store_data( frame )
    -- store some values for analysis
    frame:set_value("foot_displacement_L_y", foot_displacement)
    frame:set_value("foot_position_L_y", body:com_pos().y)
end
```

Listing 1: Lua code for minimizing vertical foot displacement.